Diagnostic Efficacy of Various Imaging Modalities Across Different Stages of Prostate Cancer: A Network Meta-Analysis of Diagnostic Studies

Chengdong Shi[1+], Kai Yu[2+], Yu Hu[3], Yuantao Wang[1], Fan Bu[4], Ji Lu[2*], Weigang Wang[1*]

1. Department of Urology II, The First Hospital of Jilin University, Changchun, Jilin, China. 130061

2. Urology Department, The First Hospital of Jilin University Changchun, Jilin, China. 130061

3. Department of Pathology, China-Japan Union Hospital of Jilin University Changchun, Jilin, China. 130061

4. Department of Plastic Surgery, The First Hospital of Jilin University, Changchun, Jilin, China. 130061

+: **Both authors contributed equally to this article.**

***Corresponding Author:** Ji Lu, PhD, Professor, Postgraduate Supervisor, Department of Urology, The First Hospital of Jilin University. Main research interests: Prostate cancer. Corresponding email: lu_ji@jlu.edu.cn

***Corresponding Author:** Weigang Wang, PhD, Professor, Postgraduate Supervisor, Department of Urology II, The First Hospital of Jilin University. Main research interests:

Prostate Cancer and Adrenal Tumors. Corresponding email: wwg@jlu.edu.cn

Abstract

Purpose: To assess the diagnostic performance of various imaging modalities in detecting and monitoring prostate cancer across different disease stages using diagnostic test accuracy (DTA) and network meta-analysis (NMA).

Methods: A systematic literature review was conducted to identify studies evaluating mpMRI, PSMA PET/CT, MRE, MRSI, BS, CT, PET, and other tracers for prostate cancer detection. Data on sensitivity, specificity, PPV, NPV, and detection rate were extracted and analyzed using NMA.

Result: Across 123 studies involving 9,371 patients, 68Ga-P16-093 PET/CT and 68Ga-PSMA-617 PET/CT showed high diagnostic accuracy in early-phase prostate cancer. For lymph node metastasis, 68Ga-PSMA-11 PET/MRI was the most sensitive. 18F-DCFPyL PET/CT had the highest specificity and PPV, while 18F-PSMA-1007 PET/CT had the highest NPV. In bone metastasis, 18F-PSMA-1007 PET/MRI excelled in sensitivity and NPV, while 18F-Fluciclovine PET/CT had the highest specificity and PPV. For biochemical recurrence, 18F-PSMA-1007 PET/CT had the highest lesion detection rate, and for different radiotracers, 18F-PSMA-1007 had the highest detection rate.

Conclusion: This network meta-analysis comprehensively evaluated the diagnostic efficacy of various imaging modalities for prostate cancer across different stages. Our findings underscore the strengths and limitations of each imaging technique in detecting and staging prostate cancer.

KEYWORDS: Prostate Cancer; PSMA PET/CT; Disease Stage; Diagnostic Test Accuracy; Network Meta-analysis

Abbreviations

ADT	Androgen Deprivation Therapy
BS	Bone Scintigraphy
BCR	Biochemical Recurrence
CAD	Computer-Aided Diagnosis
CI	Confidence Interval
CNN	Convolutional Neural Network
csPCa	Clinically Significant Prostate Cancer
CT	Computed Tomography
DCE-MRI	Dynamic Contrast-Enhanced MRI
DCFPyL	Piflufolastat
DRE	Digital Rectal Examination

DR	Detection Rate
DTA	Diagnostic Test Accuracy
DWI	Diffusion-Weighted Imaging
EAU	European Association of Urology
EANM	European Association of Nuclear Medicine
ESTRO	European Society for Radiotherapy & Oncology
ESUR	European Society of Urogenital Radiology
ECE	Extracapsular Extension
FDG	Fluoro-2-deoxy-D-glucose
FN	False Negative
FP	False Positive
ISUP	International Society of Urological Pathology
miTNM	Molecular Imaging Standardized Evaluation TNM Classification

mpMRI	Multiparametric Magnetic Resonance Imaging
MRSI	Magnetic Resonance Spectroscopy Imaging
MRE	Magnetic Resonance Elastography
NMA	Network Meta-analysis
NPV	Negative Predictive Value
OR	Odds Ratio
PCa	Prostate Cancer
PET	Positron Emission Tomography
PET/CT	Positron Emission Tomography/Computed Tomography
PET/MRI	Positron Emission Tomography/Magnetic Resonance Imaging
PI-RADS	Prostate Imaging Reporting and Data System
PPV	positive predictive value
PSA	Prostate-Specific Antigen
PSMA	Prostate-Specific Membrane Antigen

QUADAS-2	Quality Assessment of Diagnostic Accuracy Studies
RP	Radical Prostatectomy
Se	Sensitivity
Sp	Specificity
SPECT	Single Photon Emission Computed Tomography
SREs	Skeletal-Related Events
SUCRA	Surface Under Cumulative Ranking Curve
SUV	Standardized Uptake Value
SUVmax	Maximum Standardized Uptake Value
SVI	Seminal Vesicle Invasion
TP	True Positive
TN	True Negative
UBU	Unspecific Bone Uptake

1. Introduction

Prostate cancer is one of the most common malignant tumors of the male genitourinary system. According to the Global Cancer Statistics 2022 report, there were approximately 1.46 million new cases of prostate cancer in 2022, accounting for 14.2% of new cancer cases in men, making it the second most common malignancy in men after lung cancer. Additionally, there were about 390,000 new deaths due to prostate cancer, representing 7.3% of cancer-related deaths in men, ranking it fifth overall (1). Age has been identified as an independent risk factor for prostate cancer incidence (2). With the continuous growth and aging of the population, the incidence of prostate cancer is increasing annually, posing a serious threat to male health and presenting greater challenges and burdens to global public health systems (3, 4). Prostate cancer tends to exhibit subtle clinical manifestations in its early stages, leading many patients to seek medical attention only after the tumor has infiltrated or metastasized, significantly increasing mortality rates. In recent years, advancements in serology, imaging techniques, and surgical methods have contributed to higher detection rates and treatment success rates (5, 6). Among these, imaging examinations play a crucial role in screening, early diagnosis, tumor staging, surgical selection, and predicting the recurrence prognosis of prostate cancer (7, 8).

Currently, the main screening methods for prostate cancer are digital rectal examination (DRE) and serum prostate-specific antigen (PSA) testing. The introduction of PSA testing

has significantly increased the detection rate of prostate cancer. However, there is an ongoing debate about its contribution to the overdiagnosis and overtreatment of clinically insignificant tumors (9, 10). DRE has its limitations, particularly in detecting tumors located deep within the prostate or those that are smaller in size. A meta-analysis indicates that the sensitivity and specificity of DRE performed by primary care physicians are 0.51 and 0.59 (11). Therefore, the overuse of PSA testing and the low specificity and sensitivity of DRE necessitate the use of additional diagnostic methods to enhance the accuracy of prostate cancer screening. To improve tumor detection rates and achieve more accurate staging, the application of multiparametric magnetic resonance imaging (mpMRI) plays a crucial role in optimizing clinical diagnosis and biopsy procedures(12). MpMRI assesses the likelihood of tumor presence based on the Prostate Imaging Reporting and Data System (PI-RADS) and can enhance biopsy efficacy through visual guidance. A meta-analysis showed that when PI-RADS is correctly used, the pooled sensitivity for diagnosing prostate cancer is ([OR] 0.82, 95% CI [0.72-0.89]) and specificity is ([OR] 0.82, 95% CI [0.67-0.92])(13). Additionally, a study by Veeru demonstrated that compared to systematic biopsy methods, MRI-targeted biopsy (MRI-TB) has a higher detection rate for clinically significant prostate cancer ([OR] 1.16, 95% CI [1.09-1.24]) while identifying fewer cases of clinically insignificant prostate cancer (14). However, study data also show that the positive predictive value of suspicious mpMRI for clinically significant prostate cancer (csPCa) is about 40%-50%, and the negative predictive value is about 80%-90%, indicating that more than half of patients with positive mpMRI results underwent unnecessary prostate biopsies or overtreatment. Additionally, the diagnostic

sensitivity and specificity of mpMRI decrease for patients with a PI-RADS score of 3 (15, 16).

Other traditional imaging techniques, such as computed tomography (CT) and bone scintigraphy (BS), are still widely used in clinical practice, but each has its limitations. CT has low sensitivity for the initial diagnosis of prostate cancer and offers a single imaging mode, while BS is primarily used to assess bone metastasis in prostate cancer patients. Additionally, imaging modalities like magnetic resonance spectroscopy imaging (MRSI) and magnetic resonance elastography (MRE) are gradually maturing. However, these imaging techniques are generally used as auxiliary and supplementary diagnostic tools, and their cost-effectiveness and diagnostic efficiency still require further research (17).

The advent of positron emission tomography (PET) has provided a new direction for the diagnosis and treatment of prostate cancer. Initially, PET imaging used the 18F-FDG (Fluoro-2-deoxy-D-glucose) tracer, which has high sensitivity and can perform whole-body scans to detect small lesions and metastases throughout the body. Subsequently, the introduction of new tracers, such as 18F-NaF and 11C-choline, further enhanced PET's detection capabilities (18, 19). In recent years, prostate-specific membrane antigen (PSMA) PET has gained widespread recognition for its high sensitivity and specificity in diagnosing prostate cancer and assessing biochemical recurrence. PSMA is a membrane protein significantly overexpressed in prostate cancer tissue, with expression levels 100-1000 times higher than in normal prostate tissue, making it an ideal target for

molecular imaging. Increasing evidence suggests that PSMA-PET/CT and PSMA-PET/MRI have higher diagnostic efficacy than traditional imaging techniques. The diversity of PSMA ligands also provides options for addressing individual differences in prostate cancer cases. Currently, the most commonly used ligands are 68Ga-PSMA-11, 18F-DCFPyL (Piflufolastat), and 18F-PSMA-1007 (20). Meanwhile, it has been suggested that PSMA PET/CT may reduce the economic burden of high-risk patients through higher accuracy efficacy (21). However, PSMA PET is not without its limitations. Some studies indicate that while PSMA PET/CT has high specificity, its sensitivity can be inconsistent. Additionally, different tracers used in PSMA PET have varying diagnostic efficacies, and their absorption rates in different body parts can vary, raising concerns about abnormal uptake in normal or benign lesions leading to overdiagnosis and overtreatment (22). For PSMA PET/MRI, although it offers clearer contrast for soft tissues and studies have shown it to be more effective in diagnosing primary prostate cancer and biochemical recurrence (BCR) compared to mpMRI, its diagnostic performance compared to PSMA PET/CT remains unclear (23, 24) Moreover, PSMA PET/MRI is more expensive, has longer examination times, and is more challenging to implement in primary care settings.

Currently, there is controversy regarding the diagnostic performance of PSMA-PET compared to other imaging modalities and among different ligands at various stages of prostate cancer. This study aims to evaluate the diagnostic effectiveness of different imaging methods in detecting and monitoring prostate cancer at different stages by analyzing existing literature data.

2. Method

2.1 Protocol

This systematic review and meta-analysis was conducted according to the Preferred Reporting Items for Systematic Reviews and Meta-analyses (PRISMA) of diagnostic test accuracy (DTA) studies(25). The study protocol was registered on the International Prospective Register of Systematic Reviews (PROSPERO; registration ID CRD42021248896).

The aim of this systematic review is to assess the diagnostic efficacy of different imaging methods in different stages of prostate cancer. The proposed systematic review aims to answer the following questions:

i) Which imaging modality has higher diagnostic performance in the early stages of prostate cancer?

ii) Which imaging method has greater accuracy in diagnosing lymph nodes and bone metastases in prostate cancer?

iii) Which method has a higher lesion detection rate for biochemical recurrence of prostate cancer?

iv) How does the diagnostic performance of combined imaging modalities compare to individual imaging methods at different stages of prostate cancer?

2.2. Literature search

PubMed, Cochrane, and Embase were searched to identify reports published up to June 30, 2024, addressing the diagnostic value of prostate cancer at different stages (early-stage prostate cancer, advanced-stage prostate cancer, metastatic prostate cancer including bone and lymph node metastasis, recurrent prostate cancer such as biochemical recurrent prostate cancer). The keywords used in our search strategy are reported in Table 1. Initial screening was performed independently by two investigators (Shi CD and Yu K) based on the titles and abstracts of the articles to identify ineligible reports. Reasons for exclusions were noted. Potentially relevant reports were subjected to a full-text review, and the relevance of the reports was confirmed after the data extraction process. Any discrepancies during the primary and secondary literature screening were resolved by referring to the senior authors (Wang WG and Lu J).

Primary endpoint: To assess the diagnostic value of various examination methods for prostate cancer at different stages (including early-stage, advanced-stage, metastatic prostate cancer such as bone and lymph node metastasis, recurrent prostate cancer such as biochemical recurrent prostate cancer) using Diagnostic Test Accuracy meta-analysis. Since most of the patients with biochemical recurrence of prostate cancer could not be verified as true-positive or true-negative by pathology or follow-up investigations, the present study was conducted to compare the rate of lesion detection by different examination modalities in the biochemical recurrence section.

Secondary endpoint: To further evaluate the specific diagnostic value of these

examination methods in different stages of prostate cancer, including early-stage, advanced-stage, metastatic prostate cancer, and recurrent prostate cancer, and to compare their sensitivity and specificity in detecting prostate cancer at specific stages.

2.3. Inclusion and exclusion criteria

The population, intervention, control, and outcomes (PICO) for this study were determined by the co-authors as follows: Inclusion criteria: ① The content of the article is designed as a diagnostic experimental study. ② Studies need to compare the diagnostic effectiveness of two or more imaging examinations on the same patient group (mpMRI, PSMA PET, MRSI, CT, BS, PET). ③ A study that includes histopathological results or obtains pathological evidence based on clinical data, other examinations, or follow-up results. ④ Studies that include results such as true positive (TP), true negative (TN), false positive (FP), false negative (FN), sensitivity (Se), specificity (Sp), positive predictive value (PPV), negative predictive value (NPV) and detection rate (DR) or studies that can derive these results through other data calculations. If incomplete data existed for TP, TN, FP, FN, NPV, or PPV, they were calculated using the known variables Se and Sp to complete the data.

Exclusion criteria included: ① Duplicate literature; ② Non-original content such as reviews, letters to the editor, editorials, research protocols, case reports, brief communications, guidelines, and studies using other non-standard imaging modalities; ③

Studies with a sample size of fewer than ten individuals or lacking original data; ④ Non-English articles. We excluded all studies that did not evaluate the diagnostic accuracy of prostate cancer assessment in comparison to the reference method, which refers to the established standard diagnostic procedure for prostate cancer. This study focused solely on original research investigating the diagnostic accuracy of prostate biopsy, histopathological examination, and follow-up content for reported cancers, which are invasive procedures commonly used for prostate cancer diagnosis. Additionally, we excluded articles not published in English and scanned the references of all included papers for additional relevant studies.

2.4 Data extraction

Two investigators independently extracted the following information from the included articles: author, publication year, patient number, tumor stage and grade, as well as Se, Sp, and the counts of TP, FP, FN, TN, or DR for the primary outcomes. Discrepancies were resolved by consensus with coauthors.

2.5 Risk of Bias Assessment

The risk of bias in the included studies was evaluated using the revised Quality Assessment of Diagnostic Accuracy Studies tool (QUADAS-2) (26). The index test was defined as the value of Multi-Stage Prostate Cancer detection using various imaging

modalities, with prostate needle biopsy and histopathology serving as the reference standard. Discrepancies were resolved through discussion and consensus. The quality of evidence for our pooled analyses was assessed across the patient selection, index test, reference standard, and flow and timing. Each domain was assessed for risk of bias, and the first three domains were evaluated for applicability concerns.

2.6. Statistical analyses

Network meta-analysis was conducted to analyze the diagnostic accuracy of 37 imaging modalities used to detect different stages of prostate cancer, as shown in Table 2, with comparison to cytological examination. For the assessment of diagnostic accuracy, pairwise analyses were conducted to estimate the odds ratio (OR) for recurrence detection and the corresponding 95% confidence interval (CI), which were calculated from sensitivity, specificity, positive predictive value, and negative predictive value in the included manuscripts.

To assist in interpreting the diagnostic performance, the Surface Under the Cumulative Ranking Curve (SUCRA) was utilized to calculate the probability of prostate cancer at various stages, which is the best diagnostic method, employing a Bayesian approach. A higher SUCRA value indicated a superior rank for the intervention. For the consistency test, node-splitting assessments were conducted to determine the association between the direct and indirect evidence. Additionally, publication bias was evaluated using funnel plots. Stata 17.0 software was utilized for data analysis in this study.

3. Result

3.1 Study selection and characteristics

The literature search yielded 24,910 references with related content. During the screening, 8,916 articles were removed due to duplication, and 1,5132 articles were excluded for irrelevance, specific screening process in Supplementary Figure 1. Of the full-text articles assessed, 739 articles were excluded based on screening criteria.

Ultimately, after screening, a total of 123 relevant articles were included. Specifically, 38 articles were included for the diagnosis of primary prostate cancer, involving 2,182 patients; 25 articles were related to lymph node metastasis, involving 1,803 patients; 41 articles were concerned with bone metastasis, involving 3,196 patients; and 37 articles were related to biochemical recurrence of prostate cancer, involving 2,190 patients.

Supplementary Figures 2 and 3 show the results regarding the risk of bias and applicability, with red dots indicating a high risk of bias for each bias criterion, yellow dots indicating an unclear risk, and green dots indicating a low risk of bias.

3.2 Network meta-analysis of diagnostic test accuracy for prostate cancer

3.2.1 Early-phase prostate cancer

A total of 38 (23, 28-64) studies were included in this analysis. The networks of eligible comparisons are graphically represented in network plots on the diagnostic values of imaging modalities for the diagnosis of early-phase prostate cancer in Figure 1. In sensitivity comparisons, 18F-DCFBC PET/CT (Imaging14) was inferior to mpMRI (Imaging 2) (OR 0.13, 95% CI 0.02-0.75), 99mTc-PSMA SPECT/CT (Imaging 4) (OR 0.03, 95% CI 0.00-0.97), 18F-DCFPyL PET/CT (Imaging 15) (OR 0.07, 95% CI 0.01-0.61), 68Ga-P16-093 PET/CT (Imaging 29) (OR 0.01, 95% CI 0.00-0.95), and 68Ga-PSMA-11 PET/MRI (Imaging30) (OR 0.09, 95% CI 0.01-0.62). The results of the current NMA revealed that 68Ga-P16-093 PET/CT (Image29) and 68Ga-PSMA-617 PET/CT (Image33) exhibited superior diagnostic efficacy in Se, Sp, PPV and NPV, as detailed in Supplementary Figure 4.

In specificity comparisons, 18F-DCFPyL PET/CT (Imaging 15) was inferior to 18F-DCFBC PET/CT (Imaging 14) (OR 0.07, 95% CI 0.01-0.93) and 68Ga-PSMA-617 PET/CT (Imaging 33) (OR 0.05, 95% CI 0.00-0.70), while 18F-DCFPyL PET (Imaging17) was inferior to mpMRI (Imaging 2) (OR 0.02, 95% CI 0.00-0.35), 99mTc-PSMA SPECT/CT (Imaging 4) (OR 0.02, 95% CI 0.00-0.91), 18F-DCFBC PET/CT (Imaging 14) (OR 0.00, 95% CI 0.00-0.14), 18F-DCFPyL PET/MRI (Imaging 16) (OR 0.03, 95% CI 0.00-0.46), 68Ga-PSMA-11 PET/MRI (Imaging30) (OR 0.02, 95% CI 0.00-0.36), 68Ga-PSMA-11 PET/CT (Imaging 31) (OR 0.01, 95% CI 0.00-0.25), 68Ga-PSMA-11 PET (Imaging32) (OR 0.04, 95% CI 0.00-0.67), 68Ga-PSMA-617 PET/CT (Imaging 33) (OR 0.00, 95% CI 0.00-0.09), and 68Ga-RM2 PET/CT (Imaging36) (OR 0.02, 95% CI 0.00-0.50).

In positive predictive value comparisons, 18F-DCFPyL PET (Imaging 17) was inferior to mpMRI (Imaging 2) (OR 0.25, 95% CI 0.07-0.90), 68Ga-PSMA-11 PET/MRI (Imaging 30) (OR 0.19, 95% CI 0.05-0.76), 68Ga-PSMA-11 PET/CT (Imaging31) (OR 0.20, 95% CI 0.05-0.77), and 68Ga-PSMA-617 PET/CT (Imaging 33) (OR 0.06, 95% CI 0.01-0.42). 68Ga-PSMA-617 PET/CT (Imaging33) was superior to 99mTc-MDP SPECT/CT (Imaging3) (OR 68.48, 95% CI 1.35-3483.61), 18F-choline PET/CT (Imaging 11) (OR 8.70, 95% CI 1.27-59.80), 18F-DCFPyL PET/MRI (Imaging16) (OR 6.21, 95% CI 1.12-34.34), and 18F-DCFPyL PET (Imaging 17) (OR 16.60, 95% CI 2.39-115.03). There were no statistically significant differences in negative predictive value comparisons between imaging modalities and other tests, with detailed content presented in Supplementary Table 2. As such, the consistency model was applied to the current study (all $p > 0.05$).

In the analysis of SUCRA values for different imaging modalities, sensitivity was highest for 68Ga-P16-093 PET/CT (Imaging29) (84.1%), specificity was highest for 68Ga-PSMA-617 PET/CT (Imaging33) (88.1%), positive predictive value was highest for 68Ga-PSMA-617 PET/CT (Imaging33) (90.5%), and negative predictive value was highest for 68Ga-P16-093 PET/CT (Imaging 29) (80.4%). Detailed content is presented in Figure 2, which combines four plots.

3.2.1.1 Subgroup analysis: Peripheral invasion

In clinically significant prostate cancer, the primary outcome of nine studies was the diagnostic performance for csPCa. The results of the current NMA revealed that 18F-DCFPyL PET/CT (Image 15) and 68Ga-PSMA-11 PET/MRI (Image 30) exhibited superior diagnostic efficacy in Se, Sp, PPV and NPV, as detailed in the Supplementary Figure 5.

No significant statistical differences were observed in sensitivity comparisons among imaging modalities (P > 0.05). In specificity comparisons, 18F-DCFPyL PET (Image 17) was inferior to mpMRI (Image 2) (OR: 0.02, 95% CI: 0.00-0.22), 18F-DCFPyL PET/MRI (Image 16) (OR: 0.03, 95% CI: 0.00-0.34), 68Ga-PSMA-11 PET/MRI (Image 30) (OR: 0.01, 95% CI: 0.00-0.14), and 68Ga-PSMA-11 PET/CT (Image31) (OR: 0.02, 95% CI: 0.00-0.20). In positive predictive value (PPV), 18F-DCFPyL PET (Imaging 17) was weaker than mpMRI (Image 2) (OR: 0.24, 95% CI: 0.08-0.73), 68Ga-PSMA-11 PET/MRI (Image 30) (OR: 0.14, 95% CI: 0.03-0.71), and 68Ga-PSMA-11 PET/CT (Image31) (OR: 0.23, 95% CI: 0.07-0.71). No significant statistical differences were found in negative predictive value (NPV) among imaging modalities, as detailed in Supplementary Table 3

In the analysis of different imaging SUCRA values, 18F-DCFPyL PET/CT (Image15) had the highest sensitivity and NPV of 65.8 and 65.0, respectively, while 68Ga-PSMA-11 PET/MRI (Image 30) had the highest specificity and PPV of 85.0 and 83.7, respectively. The details are shown in Figure 3 (four graphs combined).

Among the studies related to extracapsular extension (ECE), a total of eight studies involved the diagnosis of ECE. The results of the current NMA revealed that mpMRI (Image 2), 18F-PSMA-1007 PET/CT (Image 21), and 68Ga-PSMA-11 PET/MRI (Image 30) exhibited superior diagnostic efficacy in Se, Sp, PPV and NPV, as detailed in the Supplementary Figure 6. No significant statistical differences were observed in sensitivity, specificity, PPV or NPV comparisons among imaging modalities. In the SUCRA values analysis, 68Ga-PSMA-11 PET/MRI (Image 30) had the highest sensitivity and NPV of 83.0 and 78.1, respectively. 18F-PSMA-1007 PET/CT (Image 21) had the highest specificity of 78.3, while mpMRI (Image 2) had the highest PPV of 62.5. The details are shown in Figure 4 (four graphs combined).

In studies related to Seminal Vesicle Invasion (SVI), the primary outcome of ten studies was the diagnosis of SVI. The results of the current NMA revealed that mpMRI (Image 2) and 18F-PSMA-1007 PET/CT (Image 21) exhibited superior diagnostic efficacy in Se, Sp, PPV and NPV, as detailed in Supplementary Figure 7.

No significant statistical differences were observed in sensitivity, specificity, PPV, or NPV comparisons among imaging modalities. In the SUCRA values analysis, 18F-PSMA-1007 PET/CT (Image 21) performed best in sensitivity, PPV, and NPV, with values of 83.3, 70.0, and 79.5, respectively. mpMRI (Image 2) performed best in specificity, with a value of 68.4. The details are shown in Figure 5 (four graphs combined).

3.2.2 lymph node metastasis

This study included 25 (28-30, 32, 46, 50, 52, 58, 59, 65-80) articles on lymph node metastasis in the initial staging of prostate cancer. The networks of eligible comparisons are graphically represented in network plots, which depict the diagnostic values of imaging examinations for the diagnosis of lymph node metastasis in prostate cancer, as shown in Figure 6. The results of the current NMA revealed that MRI (Image 1), mpMRI (Image 2), CT (Image5), 18F-DCFPyL PET/CT (Image15), 68Ga-PSMA-11 PET/MRI (Image30) and 68Ga-PSMA-11 PET/CT (Image31) showed poor diagnostic efficacy in Se, Sp, PPV and NPV, as detailed in the Supplementary Figure 8.

In the comparison of sensitivity, 68Ga-PSMA-11 PET/CT (Image 31) exhibited higher sensitivity than CT (Image 5) (OR: 4.63, 95% CI: 1.63-13.13) and mpMRI (Image 2) (OR: 3.35, 95% CI: 2.14-5.24). Additionally, 68Ga-PSMA-11 PET/CT (Image 31) demonstrated an advantage in sensitivity compared to 18F-DCFPyL PET/CT (Image 15) (OR: 4.63, 95% CI: 1.63-13.13).

However, there were no statistically significant differences in sensitivity when compared to 18F-PSMA-1007 PET/CT (Image 21), 18F-PSMA-1007 PET/MRI (Image 22), and 68Ga-PSMA-11 PET/MRI (Image 30). In the specificity analysis, 18F-DCFPyL PET/CT (Image 15) performed favorably, with higher specificity than CT (Image 5) (OR: 25.33, 95% CI: 9.00-71.25) and mpMRI (Image 2) (OR: 7.05, 95% CI: 1.86-26.63). It also showed an

advantage in specificity compared to 18F-PSMA-1007 PET/CT (Image 21) (OR: 8.71, 95% CI: 1.20-63.28), 18F-PSMA-1007 PET/MRI (Image 22) (OR: 66.28, 95% CI: 2.64-1664.42), and 68Ga-PSMA-11 PET/CT (Image 31) (OR: 10.12, 95% CI: 2.6-39.18). In the comparison of positive predictive value (PPV), 18F-DCFPyL PET/CT (Image 15) outperformed 68Ga-PSMA-11 PET/CT (Image 31) (OR: 6.29, 95% CI: 1.26-31.49), CT (OR: 16.75, 95% CI: 5.33-52.69), and mpMRI (Image 2) (OR: 8.25, 95% CI: 1.71-39.93). In the comparison of negative predictive value (NPV), 68Ga-PSMA-11 PET/CT (Image 31) was stronger than CT (Image 5) (OR: 2.53, 95% CI: 1.44-4.47) and mpMRI (Image 2) (OR: 1.48, 95% CI: 1.10-1.98), with no statistically significant differences compared to other imaging methods. Detailed data are presented in Supplementary Table 4. As such, the consistency model was applied to the current study, with all p-values > 0.05.

In the analysis of SUCRA values for different imaging modalities, 68Ga-PSMA-11 PET/MRI (Image 30) had the highest sensitivity, which was 82.9. 18F-DCFPyL PET/CT (Image 15) had the highest specificity and PPV, which were 96.4 and 90.0, respectively. 18F-PSMA-1007 PET/CT (Image 21) had the highest NPV, which was 84.1. Detailed data are presented in Figure 7, which combines four plots.

3.2.3 bone metastasis

In the analysis of bone metastases in prostate cancer, a total of 41 (28, 73, 80-118) studies were included. The networks of eligible comparisons are graphically represented

in network plots on the diagnostic values of imaging examinations for the diagnosis of bone metastases in prostate cancer in Figure 8. The results of the current NMA revealed that 99mTc-PSMA SPECT/CT (Image 4), 18F-DCFPyL PET/CT (Image 15), 18F-Fluciclovine PET/CT (Image 19), 18F-PSMA-1007 PET/CT (Image 21), 18F-PSMA-1007 PET/MRI (Image 22), 68Ga-PSMA-11 PET/MRI (Image 30) and 68Ga-PSMA-617 PET/CT (Image 33) exhibited poor diagnostic efficacy in Se, Sp, PPV and NPV, as detailed in Supplementary Figure 9.

In the sensitivity analysis, 18F-PSMA-1007 PET/MRI (Image 22) demonstrated higher sensitivity compared to 99mTc-MDP SPECT/CT (Image 4) (OR: 58.15, 95% CI: 3.19-1058.40), BS (Image 6) (OR: 142.35, 95% CI: 11.45-1769.55), 11C-choline PET/CT (Image 9) (OR: 42.29, 95% CI: 2.95-605.66), 18F-choline PET/CT (Image 11) (OR: 39.27, 95% CI: 2.55-604.24), 18F-Fluciclovine PET/CT (Image 19) (OR: 31.61, 95% CI: 1.35-740.03), 18F-NaF PET/CT (Image 20) (OR: 18.47, 95% CI: 1.27-269.18), and 68Ga-PSMA-11 PET/MRI (Image 30) (OR: 42.67, 95% CI: 1.16-1570.95), but there were no statistically significant differences when compared to 18F-PSMA-1007 PET/CT (Image 21), 18F-DCFPyL PET/CT (Image 15), and 68Ga-PSMA-617 PET/CT (Image 33). In terms of specificity, BS (Image 6) was lower than mpMRI (Image 2) (OR: 0.31, 95% CI: 0.11-0.91), 11C-choline PET/CT (Image 9) (OR: 0.15, 95% CI: 0.04-0.50), 18F-choline PET/CT (Image 11) (OR: 0.18, 95% CI: 0.05-0.68), 18F-Fluciclovine PET/CT (Image 19) (OR: 0.10, 95% CI: 0.01-0.83), and 68Ga-PSMA-11 PET/CT (Image 31) (OR: 0.14, 95% CI: 0.06-0.31). For positive predictive value comparison, 68Ga-PSMA-11 PET/CT (Image

31) was higher than mpMRI (Image 2) (OR: 2.69, 95% CI: 1.08-6.70), BS (Image 6) (OR: 6.84, 95% CI: 3.43-13.61), and 18F-NaF PET/CT (Image 20) (OR: 3.16, 95% CI: 1.16-8.60). In terms of negative predictive value, 18F-PSMA-1007 PET/MRI (Image 22) generally performed better and had advantages over other imaging methods, except for no statistically significant differences compared to 18F-PSMA-1007 PET/CT (Image 21), 68Ga-PSMA-11 PET/MRI (Image 30), 18F-Fluciclovine PET/CT (Image 19), 18F-DCFPyL PET/CT (Image 15), and 68Ga-PSMA-617 PET/CT (Image 33). The detailed content is shown in Supplementary Table 5. As such, the consistency model was applied to the current study (all $p > 0.05$).

In the SUCRA ranking plot, 18F-PSMA-1007 PET/MRI (Image 22) showed the highest sensitivity and negative predictive value of 97.4% and 95.9%, respectively. For specificity and positive predictive value, 18F-Fluciclovine PET/CT (Image 19) had the highest SUCRA values of 74.2% and 76.3%, respectively. The detailed content is shown in Figure 9 (four plots together).

3.2.3.1 Subgroup Analysis Newly Diagnosed and Biochemically Recurrent Prostate Cancer

The studies included in the bone metastasis analysis were categorized into two groups based on disease stage: newly diagnosed and biochemically recurrent prostate cancer. The remaining studies involved a mixed analysis of biochemical recurrence and newly

diagnosed and were not included in the subgroup analysis. Additionally, due to the unknown initial treatment types and androgen deprivation therapy (ADT) proportions in the studies involving biochemical recurrence patients, relevant subgroup analysis could not be conducted.

In newly diagnosed prostate cancer bone metastases, a total of 17 studies were included. The results of the current NMA revealed that mpMRI (Image 2), 18F-DCFPyL PET/CT (Image 15), 18F-PSMA-1007 PET/MRI (Image 22), 68Ga-PSMA-11 PET/MRI (Image 30), 68Ga-PSMA-11 PET/CT (Image 31), 68Ga-PSMA-11 PET (Image 32) and 68Ga-PSMA-617 PET/CT (Image 33) exhibited poor diagnostic efficacy in Se, Sp, PPV and NPV, as detailed in Supplementary Figure 10. For sensitivity comparisons, the sensitivity of BS (Image 6) was lower than that of 18F-choline PET/CT (Image 11) (OR: 0.20, 95% CI: 0.06-0.68), 18F-DCFPyL PET/CT (Image 15) (OR: 0.06, 95% CI: 0.01-0.72), 18F-NaF PET/CT (Image 20) (OR: 0.13, 95% CI: 0.04-0.42), 18F-PSMA-1007 PET/MRI (Image 22) (OR: 0.03, 95% CI: 0.00-0.61), and 68Ga-PSMA-11 PET/CT (Image 31) (OR: 0.11, 95% CI: 0.03-0.47). However, there was no statistical difference compared to mpMRI (Image 2) (OR: 0.09, 95% CI: 0.01-1.16) and 99mTc-MDP SPECT/CT (Image 3) (OR: 0.33, 95% CI: 0.06-1.90). In terms of specificity, BS (Image 6) specificity was lower than that of mpMRI (Image 2) (OR: 0.13, 95% CI: 0.02-0.89), 99mTc-MDP SPECT (Image 7) (OR: 0.08, 95% CI: 0.01-0.53), and 68Ga-PSMA-11 PET/CT (Image 31) (OR: 0.14, 95% CI: 0.04-0.45). Similar to specificity, BS (Image 6) was lower than mpMRI (Image 2), 99mTc-MDP SPECT (Image 7), and 68Ga-PSMA-11 PET/CT (Image 31) in positive

predictive value. When comparing negative predictive values, BS (Image 6) was lower than other imaging methods except for 68Ga-PSMA-617 PET/CT (Image 33), mpMRI (Image 2), and 99mTc-MDP SPECT/CT (Image 3). Specific details are shown in Supplementary Table 6. As such, the consistency model was applied to the current study (all $p > 0.05$).

In the analysis of SUCRA values for different imaging techniques, 68Ga-PSMA-11 PET (Image 32) showed the best performance in sensitivity and negative predictive value, with values of 86.6% and 85.9%, respectively. 99mTc-MDP SPECT (Image 3) had the highest specificity of 82.3%. mpMRI (Image 2) showed the highest positive predictive value of 82.1%. Specific details are shown in Figure 10.

In biochemically recurrent prostate cancer bone metastases, a total of 17 studies were included. The results of the current NMA revealed that mpMRI (Image 2), BS (Image 6), 11C-choline PET/CT (Image 9) and 68Ga-PSMA-11 PET/CT (Image 31) exhibited poor diagnostic efficacy in Se, Sp, PPV and NPV, as detailed in the Supplementary Figure 11. No statistical difference was found in sensitivity and negative predictive value comparisons between imaging examinations. In terms of specificity, BS (Image 6) was lower than mpMRI (Image 2) (OR: 0.20, 95% CI: 0.06-0.70), 11C-choline PET/CT (Image 9) (OR: 0.10, 95% CI: 0.03-0.31), and 68Ga-PSMA-11 PET/CT (Image 31) (OR: 0.16, 95% CI: 0.06-0.44). In positive predictive value comparisons, BS (Image 6) was lower than 11C-choline PET/CT (Image 9) (OR: 0.13, 95% CI: 0.04-0.41) and 68Ga-PSMA-11

PET/CT (Image 31) (OR: 0.17, 95% CI: 0.06-0.48), with no significant statistical difference compared to other imaging methods. Specific details are shown in Supplementary Table 7. As such, the consistency model was applied to the current study (all p > 0.05).

In the SUCRA ranking chart, 18F-NaF PET/CT (Image 20) showed the highest sensitivity of 79.5%. In terms of specificity, 68Ga-PSMA-11 PET (Image 32) had the highest SUCRA value of 83.8%. For positive predictive value and negative predictive value, 18F-Fluciclovine PET/CT (Image 19) and MRI (Image 1) performed best, with values of 78.6% and 85.1%, respectively. Specific details are shown in Figure 11.

3.2.4 biochemical recurrence

In the investigation of biochemical recurrence, a total of 37 (28, 102, 108-110, 112, 119-149) studies were included. The networks of eligible comparisons are graphically represented in network plots, showcasing the diagnostic values of imaging examinations for the diagnosis of biochemical recurrence of prostate cancer in Figure 12. Notably, 68Ga-NeoB PET/MRI (Image 28) and 68Ga-PSMA-R2 PET/MRI (Image 35) did not form network relationships with other diagnostic methods and were therefore excluded from subsequent analyses. The results of the current NMA revealed that mpMRI (Image 2), BS (Image 6), 11C-choline PET/CT (Image 9) and 68Ga-PSMA-11 PET/CT (Image 31) were poor in terms of lesion detection rates, as detailed in the Supplementary Table 8. Ranked by SUCRA values, 18F-PSMA-1007 PET/CT (Image 21) exhibited the best performance

in detecting biochemical recurrence, with a rate of 98.1. The specific details are illustrated in Figure 13.

3.2.4.1 Subgroup Analysis: Radioactive Markers

Furthermore, this study conducted an additional analysis and comparison of the detection rates of biochemical recurrence in prostate cancer, classified according to radioactive tracers. Notably, two radioactive tracers, 68Ga-PSMA-R2 and 68Ga-NeoB, did not form network relationships with other tracers and were therefore excluded from subsequent analyses. The estimated scanning rate ratios for pairwise comparisons among the radioactive markers in the NMA are presented in Supplementary Table 9. Ranked by SUCRA values, 18F-PSMA-1007 exhibited the best performance in detecting biochemical recurrence, with a rate of 98.8. The detection rates of 64Cu-PSMA-617, 68Ga-PSMA-11, and 18F-DCFPyL were comparable, with rates of 74.9, 70.0, and 66.3, respectively. The specific details are illustrated in Figure 14.

3.3 Bias analysis: Small sample effect estimation

Funnel plots were drawn for the total effective outcome indicator to test for publication bias. The results showed that all studies were generally symmetrically distributed around the X = 0 vertical line, and most studies fell inside the funnel, whereas some fell at the bottom, suggesting a possible small sample effect (Figure 15).

4. Discussion

In this systematic review and network meta-analysis, we comprehensively evaluated the diagnostic efficacy of various imaging modalities for prostate cancer at different stages, including early-phase, lymph node metastasis, bone metastasis, and biochemical recurrence. Our findings highlight the strengths and limitations of each imaging technique in detecting and staging prostate cancer.

The 5-year survival rate of prostate cancer is highly correlated with tumor staging, and improving the accuracy of early diagnosis can significantly enhance patient survival rates (150). In the early diagnosis of prostate cancer, mpMRI is recommended before biopsy, and patients with PI-RADS ≤ 2 may be exempted from prostate cancer biopsy (151). Prostate-specific membrane antigen (PSMA) is a type 2 transmembrane glycoprotein that provides necessary metabolic substrates for cancer cell proliferation and invasion by mediating folate hydrolysis (152). In high-grade metastatic prostate cancer, particularly in aggressive, androgen-deprived, metastatic, and hormone-refractory PCa, PSMA expression is significantly increased and is currently the main target for detecting minimal prostate cancer lesions (153, 154). PSMA mediates folate hydrolysis, providing essential metabolic substrates for cancer cell proliferation and invasion.

PET/CT tracers primarily encompass three functionalities: detecting cell division activity

(such as radiolabeled choline, acetate, fluorodeoxyglucose, amino acids), targeting cancer-specific membrane proteins or receptors (like prostate-specific membrane antigen, gastrin-releasing peptide receptors), and compounds specifically binding to bone metastases (e.g., radiolabeled sodium fluoride) (155). Due to PSMA's involvement in the PI3K/AKT growth pathway related to prostate cancer metastasis (156), PSMA-PET can better reflect the overall tumor burden in the body (157).

The PSMA/PET evaluation system integrates PSMA expression V (based on background contrast) and PSMA expression Q (using SUV values), where significantly higher PSMA expression than the liver is considered a typical pathological feature of prostate cancer (158). This system demonstrates higher SUVmax values in more aggressive tumors, further confirming its diagnostic efficacy (159). Multi-Parametric MRI (mpMRI) combines anatomical imaging (such as T2-weighted MRI, which differentiates anatomical structures based on water molecule relaxation time differences and possesses excellent spatial resolution) with functional imaging (including Diffusion-Weighted Imaging (DWI) to assess water molecule diffusion in tissue structures, where tumor regions appear as high signals; and DCE-MRI to evaluate angiogenesis and perfusion characteristics through contrast agent injection, providing information on tumor blood supply) (160). Studies have shown that the combined use of mpMRI and PSMA PET/CT significantly improves the negative predictive value and sensitivity of diagnosis (31), which may be related to the targeted biopsy capabilities of PSMA PET/CT for patients with metal implants. In the imaging diagnosis of prostate cancer, MRI-TRUS fusion imaging has become a clinically preferred

option (7).

Establishing a high-precision diagnostic method for early-stage prostate cancer is crucial for reducing unnecessary biopsies and the associated risks of overtreatment and invasive injuries to patients. Current research indicates that Digital Rectal Examination (DRE) performs poorly in early screening for prostate cancer, potentially increasing the risk of overtreatment and unnecessary physical harm (11, 161). Particularly in middle-aged men, the diagnostic efficacy of DRE is inferior to PSA screening. Therefore, screening and diagnostic strategies for prostate cancer should comprehensively consider patients' expected lifespan and health status. According to the EAU-EANM-ESTRO-ESUR-ISUP-SIOG guidelines, local treatment is recommended for patients with an expected lifespan exceeding ten years, while those with a shorter lifespan (e.g., <10 to 15 years) may be more suitable for active surveillance or androgen deprivation therapy (162).

The accuracy of mpMRI (multiparametric magnetic resonance imaging) in early diagnosis of prostate cancer is highly dependent on the professional expertise of imaging specialists. However, with the deep integration of computer science and medical imaging technology, particularly the application of advanced computer-aided diagnosis (CAD) techniques such as Convolutional Neural Networks (CNNs), the precision of mpMRI in the early detection of prostate cancer has been significantly enhanced (163). This advancement provides strong technical support for the early and precise diagnosis of prostate cancer.

In advanced cases, bone metastasis is one of the leading causes of death (164). Planar bone scintigraphy (BS) using Technetium-99m (99mTc) diphosphonates is currently a primary imaging modality for assessing high-risk prostate cancer, characterized by low cost, high sensitivity, and low specificity (165). Bone activation induced by hormonal therapy can result in heterogeneous bone uptake, masking bone metastasis(166). False positives mainly occur in noncancerous bone conditions of the spine and ribs (91).

The axial skeleton is the primary site of skeletal-related events (SREs) in prostate cancer (167). In the diagnosis of advanced disease, PSMA PET/CT demonstrates higher accuracy, lower radiation exposure, and fewer equivocal diagnostic lesions compared to traditional imaging modalities such as CT and bone scans (168), as well as higher interobserver agreement (169). In the selection of molecular hybrid imaging ligands, 18F-PSMA-1007 is primarily eliminated via the hepatobiliary route, while 68Ga-PSMA-11 is excreted through both the hepatobiliary and urinary systems; thus 18F-PSMA-1007 exhibits better diagnostic performance (170), especially in lesions around the bladder (171), unspecific bone uptake (UBU) (172), and soft tissue surrounding the lesion (90). Delayed imaging can be used to increase diagnostic accuracy in patients with high bladder urine activity (173).

In the assessment of single bone metastasis lesions, 18F-NaF PET/CT demonstrates superiority over 68Ga-PSMA PET/CT (174). This is attributed to its longer half-life (175)

and higher interobserver agreement (176). Compared to PET/CT, PET/MRI exhibits greater sensitivity in the early diagnosis of bone metastases, albeit with a higher economic burden (177). Muehlematter et al. found that PSMA-PET/MRI is more sensitive than mpMRI in detecting extracapsular extension and seminal vesicle invasion in prostate cancer (45). PSMA PET also reveals the expression of PSMA in tumor-related metastatic lesions, providing a basis for potential PSMA radioligand therapy (178). Studies have also shown that 99mTc-PSMA SPECT/CT outperforms 99mTc (Methylene Diphosphonate)-MDP SPECT/CT in diagnosing bone metastases in patients with small lesions or low PSA levels. Due to differences in PSA diagnostic thresholds (99mTc-PSMA SPECT/CT: 2.635 ng/mL; 99mTc-MDP SPECT/CT: 15.275 ng/mL) and late imaging, 99mTc-PSMA SPECT/CT remains the preferred choice for patients with low PSA levels (115, 179). In assessing metastatic prostate cancer (mPCa), PSMA PET/CT defines significant increases in PSMA uptake or a >30% increase in tumor PET volume as criteria for disease progression, effectively curbing overtreatment of non-clearly progressive prostate cancer (180).

After primary treatment, biochemical recurrence (BCR) of prostate Cancer may occur, which can be classified as a negative or fossa-confined disease, lymph nodal, or distant metastatic disease. The three-year recurrence-free rate gradually decreases among these patients (181). Accurate tumor localization is crucial for guiding subsequent salvage therapies (175). Approximately 40% of patients may experience biochemical recurrence within five years after definitive treatment (182). Among patients with biochemical

recurrence, 24%-34% will develop overt metastatic disease within 15 years after surgery (183). BCR is defined as a rise in PSA levels to ≥0.2 ng/ml in patients treated with radical prostatectomy or an increase in PSA to ≥2 ng/ml above the nadir in the case of primary radiotherapy, in accordance with the Phoenix criteria(184). In some cases of recurrent prostate cancer within the prostatic fossa, diagnostic accuracy can be improved by the administration of furosemide (185).

When detecting lymph node metastasis in radical prostatectomy, PSMA PET/CT exhibits high sensitivity and specificity for lymph nodes larger than 5mm (186). The primary manifestation of prostate cancer recurrence after radical prostatectomy is the presence of early enhancement foci confined to the prostatic fossa (fossa-confined disease). Post-treatment, the Prostate Imaging Reporting and Data System (PI-RADS) is no longer applicable, regardless of whether the prostate cancer was treated surgically or with primary therapy (187). Diffusion-weighted imaging-Magnetic Resonance Imaging (DWI-MRI) is the most accurate sequence for detecting prostate cancer recurrence (188). When diagnosing BCR, PSMA exhibits higher sensitivity and specificity compared to 18F-choline and 18F-fluciclovine, which rely heavily on PSA levels (123, 189).

The primary site of prostate cancer recurrence is at the bladder-ureter anastomosis, followed by the anterior or posterior bladder neck. In the diagnosis of local recurrence, PET-MRI demonstrates better recognition than PET-CT (190). 18F-PSMA-1007 PET/CT is highly specific for diagnosing lymph node recurrence after radical prostatectomy (RP),

with a specificity of up to 99% (176, 191). Radiocomposites, such as 18F-NOTA-GRPR-PSMA, may represent a future direction for enhancing diagnostic efficacy (191). PSMA-PET exhibits high sensitivity for patients with high PSA levels, high Gleason scores, and rapid PSA doubling time (PSA-DT) (192). As PSMA PET/CT can be influenced by the androgen signaling pathway, it is typically recommended to wait at least three months after initiating ADT or second-generation anti-androgen therapy before performing a PSMA PET/CT scan (193).

This network meta-analysis offers a comprehensive evaluation of the diagnostic efficacy of diverse imaging modalities in the detection and staging of prostate cancer across various stages, including early-phase disease, lymph node metastasis, bone metastasis, and biochemical recurrence. Our findings emphatically highlight the strengths and limitations of each imaging technique in the context of prostate cancer detection and staging. However, due to limitations in medical and economic resources, a subset of patients remains unable to access more precise imaging modalities. As a result, high-precision examinations are often reserved for patients with advanced or overtly progressing diseases.

This study is also subject to several limitations. Firstly, the utilization of varying reference standards for different aspects of the study, along with the acquisition of some data through follow-up, may potentially impact the research findings. Secondly, the existence of potential publication bias, whereby some negative results may remain unpublished due

to their non-significance, could also influence the research outcomes. Furthermore, the fact that some studies did not directly report raw data, with some data instead derived through calculations, may introduce discrepancies compared to the original data. Additionally, factors such as varying ethnic groups, different clinical scenarios, and the absence of long-term follow-up for emerging technologies can also exert an impact on the results. Finally, this study analyzed the efficacy of specific imaging methods for the diagnosis of prostate cancer. In the included literature, certain imaging methods were less well documented or involved a smaller total number of patients, and there may have been some bias when they were compared with each other. Consequently, further exploration of this issue necessitates multi-center, large-sample studies to gain a deeper understanding.

5. Conclusion

Our study contributes to the guidance of imaging modalities for prostate cancer across various stages. By utilizing appropriate imaging techniques, we have mitigated the potential harm caused by invasive procedures to patients. Additionally, we have provided cost-effective imaging methods for managing potential multi-stage prostate cancer conditions, thereby reducing the financial burden on patients during their medical journey. With the continuous development of ligands, precise diagnosis for an even wider range of prostate cancer stages, at a more granular level, will become a reality in the future.

Appendix

Competing interests

The authors declare that the research was conducted in the absence of any commercial or financial relationships that could be construed as a potential conflict of interest.

Data availability statement

The original contributions presented in the study are included in the article/Supplementary Material. Further inquiries can be directed to the corresponding author.

Funding

This study was supported by Jilin Scientific and Technological Development Program (20200201315JC), Natural Science Foundation of Jilin Province (20210101272JC), Jilin Province Tianhua Health Foundation (J2023JKJ017), Beijing Bethune Charity Foundation (mnzl202022) and Key Research and Development Project in the field of medicine and health of Jilin Provincial Department of Science and Technology (20230204091YY) .

Acknowledgements

Thanks for all the patients in this research, and thanks for all the scholars in this article. Thanks for all the teammates for supporting this research. This work was financially supported by Research project of the Science and Technology Development Project of Jilin Province, China (20200201315JC) . We are also particularly grateful to our colleagues in The First Affiliated Hospital of Jilin University for their contributions.

Author contributions

CD S and KY: Study design, literature search and manuscript writing. YH and YT W: Study selection and data analysis. CD S and KY: Data collection. WG W and JL: Article Guidance. All authors revised the manuscript, approved the final manuscript as submitted, and agreed to take responsibility for all aspects of the work.

Publisher's note

All claims expressed in this article are solely those of the authors and do not necessarily represent those of their affiliated organizations or those of the publisher, the editors and the reviewers. Any product that may be evaluated in this article or claim that may be made by its manufacturer is not guaranteed or endorsed by the publisher.

Figure Legend

Figure 1:

- **Title**: Network plots on the diagnostic values of imaging modalities for the diagnosis of early-phase prostate cancer.
- **Description**: This figure displays the network of eligible comparisons graphically, illustrating the diagnostic values of various imaging modalities used for the detection of early-phase prostate cancer.

Figure 2:

- **Title**: SUCRA values for different imaging modalities in early-phase prostate

cancer diagnosis based on sensitivity, specificity, positive predictive value (PPV), and negative predictive value (NPV).

- **Description**: This figure presents the Surface Under the Cumulative Ranking Curve (SUCRA) values for various imaging modalities, indicating their relative diagnostic performance in early-phase prostate cancer detection based on sensitivity, specificity, PPV, and NPV.

Figure 3:

- **Title**: SUCRA values for different imaging modalities in clinically significant prostate cancer diagnosis based on sensitivity, specificity, positive predictive value (PPV), and negative predictive value (NPV).
- **Description**: This figure presents the Surface Under the Cumulative Ranking Curve (SUCRA) values for various imaging modalities, indicating their relative diagnostic performance in clinically significant prostate cancer detection based on sensitivity, specificity, PPV, and NPV.

Figure 4:

- **Title**: SUCRA values for different imaging modalities in extracapsular extension prostate cancer diagnosis based on sensitivity, specificity, positive predictive value (PPV), and negative predictive value (NPV).
- **Description**: This figure presents the Surface Under the Cumulative Ranking Curve (SUCRA) values for various imaging modalities, indicating their relative

diagnostic performance in extracapsular extension prostate cancer detection based on sensitivity, specificity, PPV, and NPV.

Figure 5:

- **Title**: SUCRA values for different imaging modalities in seminal vesicle invasion prostate cancer diagnosis based on sensitivity, specificity, positive predictive value (PPV), and negative predictive value (NPV).
- **Description**: This figure presents the Surface Under the Cumulative Ranking Curve (SUCRA) values for various imaging modalities, indicating their relative diagnostic performance in seminal vesicle invasion prostate cancer detection based on sensitivity, specificity, PPV, and NPV.

Figure 6:

- **Title**: Network plots on the diagnostic values of imaging modalities for the diagnosis of lymph node metastasis prostate cancer.
- **Description**: This figure displays the network of eligible comparisons graphically, illustrating the diagnostic values of various imaging modalities used for the detection of lymph node metastasis prostate cancer.

Figure 7:

- **Title**: SUCRA values for different imaging modalities in lymph node metastasis prostate cancer diagnosis based on sensitivity, specificity, positive predictive

value (PPV), and negative predictive value (NPV).

- **Description**: This figure presents the Surface Under the Cumulative Ranking Curve (SUCRA) values for various imaging modalities, indicating their relative diagnostic performance in lymph node metastasis prostate cancer detection based on sensitivity, specificity, PPV, and NPV.

Figure 8:

- **Title**: Network plots on the diagnostic values of imaging modalities for the diagnosis of bone metastasis prostate cancer.
- **Description**: This figure displays the network of eligible comparisons graphically, illustrating the diagnostic values of various imaging modalities used for the detection of bone metastasis prostate cancer.

Figure 9:

- **Title**: SUCRA values for different imaging modalities in bone metastasis prostate cancer diagnosis based on sensitivity, specificity, positive predictive value (PPV), and negative predictive value (NPV).
- **Description**: This figure presents the Surface Under the Cumulative Ranking Curve (SUCRA) values for various imaging modalities, indicating their relative diagnostic performance in bone metastasis prostate cancer detection based on sensitivity, specificity, PPV, and NPV.

Figure 10:

- **Title**: SUCRA values of different imaging modalities based on sensitivity, specificity, positive predictive value (PPV) and negative predictive value (NPV) in the diagnosis of bone metastases in newly diagnosed prostate cancer.
- **Description**: This figure presents the Surface Under the Cumulative Ranking Curve (SUCRA) values for various imaging modalities, indicating their relative diagnostic performance in the detection of bone metastases in newly diagnosed prostate cancer based on sensitivity, specificity, PPV, and NPV.

Figure 11:

- **Title**: SUCRA values of different imaging modalities based on sensitivity, specificity, positive predictive value (PPV) and negative predictive value (NPV) in the diagnosis of biochemically recurrent prostate cancer bone metastases.
- **Description**: This figure presents the Surface Under the Cumulative Ranking Curve (SUCRA) values for various imaging modalities, indicating their relative diagnostic performance in the detection of biochemically recurrent prostate cancer bone metastases based on sensitivity, specificity, PPV, and NPV.

Figure 12:

- **Title**: Network plots on the diagnostic values of imaging modalities for the diagnosis of biochemical recurrence cancer.
- **Description**: This figure displays the network of eligible comparisons graphically,

illustrating the diagnostic values of various imaging modalities used for the detection of biochemical recurrence of prostate cancer.

Figure 13:

- **Title**: SUCRA values for different imaging modalities in biochemical recurrence of prostate cancer diagnosis based on detection rate (DR).
- **Description**: This figure presents the Surface Under the Cumulative Ranking Curve (SUCRA) values for various imaging modalities, indicating their relative diagnostic performance in biochemical recurrence of prostate cancer detection based on detection rate (DR).

Figure 14:

- **Title**: SUCRA values for different radiotracers in the diagnosis of biochemical recurrence of prostate cancer based on detection rate (DR).
- **Description**: This figure presents the Surface Under the Cumulative Ranking Curve (SUCRA) values for various radiotracers, indicating their relative diagnostic performance in biochemical recurrence of prostate cancer detection based on detection rate (DR).

Figure 15:

- **Title**: Funnel plots of various imaging modalities for different stages of prostate cancer.

- **Description**: (A) Funnel plot of early prostate cancer; (B) Funnel plot of clinically significant prostate cancer; (C) Funnel plot of extracapsular extension; (D) Funnel plot of seminal vesicle invasion; (E) Funnel plot of lymph node metastasis; (F) Funnel plot of bone metastasis; (G) Funnel plot of bone metastases in newly diagnosed prostate cancer; (H) Funnel plot of bone metastases in biochemically recurrent prostate cancer; (I) Funnel plot of biochemical recurrence of prostate cancer; (J) Funnel plot of biochemically recurrent prostate cancer with different radiotracers.

Table Legend

Table 1:

- **Title**: Keywords used in the literature search strategy.
- **Description**: This table lists the keywords used in the literature search to identify relevant studies for the systematic review and meta-analysis.

Table 2:

- **Title**: Overview of imaging modalities included in the network meta-analysis.
- **Description**: This table provides an overview of the different imaging modalities considered in the network meta-analysis, including their abbreviations and full names.

Supplementary Materials Legend

Supplementary Figure 1:

- **Title**: Literature screening process and its corresponding results.
- **Description**: This supplementary figure illustrates the literature screening process and the number of articles included or excluded at each stage of the screening process.

Supplementary Figure 2:

- **Title**: QUADAS 2 individual study results. A: Results of quality assessment of early-phase prostate cancer; B: Results of quality assessment of lymph node metastasis in prostate cancer; C: Results of quality assessment of bone metastases from prostate cancer; D: Results of quality assessment of biochemically recurrent prostate cancer.

Supplementary Figure 3:

- **Title**: Overall summary bar graphs of risk of bias and applicability concerns across studies using the Quality Assessment of Diagnostic Accuracy Studies-2 (QUADAS-2). A: Results of quality assessment of early-phase prostate cancer; B: Results of quality assessment of lymph node metastasis in prostate cancer; C: Results of quality assessment of bone metastases from prostate cancer; D: Results of quality assessment of biochemically recurrent prostate cancer.

Supplementary Figure 4:

- **Title**: Forest plots of early-phase prostate cancer

Supplementary Figure 5:

- **Title**: Forest plots of clinically significant prostate cancer

Supplementary Figure 6:

- **Title**: Forest plots of extracapsular extension of prostate cancer

Supplementary Figure 7:

- **Title**: Forest plots of seminal vesicle invasion of prostate cancer

Supplementary Figure 8:

- **Title**: Forest plots of lymph node metastasis of prostate cancer

Supplementary Figure 9:

- **Title**: Forest plots of bone metastasis of prostate cancer

Supplementary Figure 10:

- **Title**: Forest plots of bone metastases in newly diagnosed prostate cancer

Supplementary Figure 11:

- **Title**: Forest plots of bone metastases in biochemically recurrent prostate cancer

Supplementary Table 1:

- **Title**: Characteristics of studies reporting imaging modalities for the diagnosis of prostate cancer at various stages.
- **Description**: This supplementary table provides detailed characteristics of studies included in the systematic review, organized by the stage of prostate cancer (early-phase, lymph node metastasis, bone metastasis, biochemical recurrence).
-

Supplementary Table 2:

- **Title**: Detailed results of pairwise comparisons in the network meta-analysis for early-phase prostate cancer diagnosis.
- **Description**: This supplementary table presents detailed results of pairwise comparisons between imaging modalities in the network meta-analysis for early-phase prostate cancer diagnosis.
-

Supplementary Table 3:

- **Title**: Detailed results of pairwise comparisons in the network meta-analysis for clinically significant prostate cancer
- **Description**: This supplementary table provides detailed results of pairwise comparisons between imaging modalities in the network meta-analysis for lymph

node metastasis detection in prostate cancer.

Supplementary Table 4:

- **Title**: Detailed results of pairwise comparisons in the network meta-analysis for lymph node metastasis diagnosis.
- **Description**: This supplementary table provides detailed results of pairwise comparisons between imaging modalities in the network meta-analysis for lymph node metastasis detection in prostate cancer.
-

Supplementary Table 5:

- **Title**: Detailed results of pairwise comparisons in the network meta-analysis for bone metastasis diagnosis.
- **Description**: This supplementary table outlines detailed results of pairwise comparisons between imaging modalities in the network meta-analysis for bone metastasis detection in prostate cancer.

Supplementary Table 6:

- **Title**: Detailed results of pairwise comparisons in the network meta-analysis for bone metastases in newly diagnosed prostate cancer.
- **Description**: This supplementary table presents detailed results of pairwise comparisons between imaging modalities in the network meta-analysis for bone metastases in newly diagnosed prostate cancer.

Supplementary Table 7:

- **Title**: Detailed results of pairwise comparisons in the network meta-analysis for bone metastases in biochemically recurrent prostate cancer.
- **Description**: This supplementary table presents detailed results of pairwise comparisons between imaging modalities in the network meta-analysis for bone metastases in biochemically recurrent prostate cancer.

Supplementary Table 8

- **Title**: Detailed results of pairwise comparisons in the network meta-analysis for biochemical recurrence prostate cancer.
- **Description**: This supplementary table presents detailed results of pairwise comparisons between imaging modalities in the network meta-analysis for biochemical recurrence of prostate cancer.

Supplementary Table 9

- **Title**: Detailed results of pairwise comparisons in the network meta-analysis for in detection rates of biochemical recurrence in prostate cancer, classified according to radioactive tracers.
- **Description**: This supplementary table presents detailed results of pairwise comparisons between imaging modalities in the network meta-analysis for detection rates of biochemical recurrence in prostate cancer, classified according

to radioactive tracers.

References

1. Bray F, Laversanne M, Sung H, Ferlay J, Siegel RL, Soerjomataram I, et al. Global cancer statistics 2022: GLOBOCAN estimates of incidence and mortality worldwide for 36 cancers in 185 countries. CA Cancer J Clin. 2024;74(3):229-63.

2. Bergengren O, Pekala KR, Matsoukas K, Fainberg J, Mungovan SF, Bratt O, et al. 2022 Update on Prostate Cancer Epidemiology and Risk Factors-A Systematic Review. Eur Urol. 2023;84(2):191-206.

3. Mumuni S, O'Donnell C, Doody O. The Risk Factors and Screening Uptake for Prostate Cancer: A Scoping Review. Healthcare (Basel). 2023;11(20).

4. Zhang W, Cao G, Wu F, Wang Y, Liu Z, Hu H, et al. Global Burden of Prostate Cancer and Association with Socioeconomic Status, 1990-2019: A Systematic Analysis from the Global Burden of Disease Study. J Epidemiol Glob Health. 2023;13(3):407-21.

5. Pastor-Navarro B, Rubio-Briones J, Borque-Fernando Á, Esteban LM, Dominguez-Escrig JL, López-Guerrero JA. Active Surveillance in Prostate Cancer: Role of Available Biomarkers in Daily Practice. Int J Mol Sci. 2021;22(12).

6. Van Poppel H, Albreht T, Basu P, Hogenhout R, Collen S, Roobol M. Serum PSA-based early detection of prostate cancer in Europe and globally: past, present and future. Nat Rev Urol. 2022;19(9):562-72.

7. Schlemmer HP, Krause BJ, Schütz V, Bonekamp D, Schwarzenböck SM, Hohenfellner M. Imaging of Prostate Cancer. Dtsch Arztebl Int. 2021;118(42):713-9.

8. Eldred-Evans D, Tam H, Sokhi H, Padhani AR, Connor M, Price D, et al. An Evaluation of Screening Pathways Using a Combination of Magnetic Resonance Imaging and Prostate-specific Antigen: Results from the IP1-PROSTAGRAM Study. Eur Urol Oncol. 2023;6(3):295-302.

9. Kachuri L, Hoffmann TJ, Jiang Y, Berndt SI, Shelley JP, Schaffer KR, et al. Genetically adjusted PSA levels for prostate cancer screening. Nat Med. 2023;29(6):1412-23.

10. Vickers A, O'Brien F, Montorsi F, Galvin D, Bratt O, Carlsson S, et al. Current policies on early detection of prostate cancer create overdiagnosis and inequity with minimal benefit. Bmj. 2023;381:e071082.

11. Naji L, Randhawa H, Sohani Z, Dennis B, Lautenbach D, Kavanagh O, et al. Digital Rectal Examination for Prostate Cancer Screening in Primary Care: A Systematic Review and Meta-Analysis. Ann Fam Med. 2018;16(2):149-54.

12. Padhani AR, Schoots IG. Prostate cancer screening-stepping forward with MRI. Eur Radiol. 2023;33(10):6670-6.

13. Hamoen EHJ, de Rooij M, Witjes JA, Barentsz JO, Rovers MM. Use of the Prostate Imaging Reporting and Data System (PI-RADS) for Prostate Cancer Detection with Multiparametric Magnetic Resonance Imaging: A Diagnostic Meta-analysis. Eur Urol. 2015;67(6):1112-21.

14. Kasivisvanathan V, Stabile A, Neves JB, Giganti F, Valerio M, Shanmugabavan Y, et al. Magnetic Resonance Imaging-targeted Biopsy Versus Systematic Biopsy in the Detection of Prostate Cancer: A Systematic Review and Meta-analysis. Eur Urol. 2019;76(3):284-303.

15. Mazzone E, Stabile A, Pellegrino F, Basile G, Cignoli D, Cirulli GO, et al. Positive

Predictive Value of Prostate Imaging Reporting and Data System Version 2 for the Detection of Clinically Significant Prostate Cancer: A Systematic Review and Meta-analysis. Eur Urol Oncol. 2021;4(5):697-713.

16. Sathianathen NJ, Omer A, Harriss E, Davies L, Kasivisvanathan V, Punwani S, et al. Negative Predictive Value of Multiparametric Magnetic Resonance Imaging in the Detection of Clinically Significant Prostate Cancer in the Prostate Imaging Reporting and Data System Era: A Systematic Review and Meta-analysis. Eur Urol. 2020;78(3):402-14.

17. Seitz M, Shukla-Dave A, Bjartell A, Touijer K, Sciarra A, Bastian PJ, et al. Functional magnetic resonance imaging in prostate cancer. Eur Urol. 2009;55(4):801-14.

18. Li R, Ravizzini GC, Gorin MA, Maurer T, Eiber M, Cooperberg MR, et al. The use of PET/CT in prostate cancer. Prostate Cancer Prostatic Dis. 2018;21(1):4-21.

19. Picchio M, Briganti A, Fanti S, Heidenreich A, Krause BJ, Messa C, et al. The role of choline positron emission tomography/computed tomography in the management of patients with prostate-specific antigen progression after radical treatment of prostate cancer. Eur Urol. 2011;59(1):51-60.

20. Alberts IL, Seifert R, Werner RA, Rowe SP, Afshar-Oromieh A. Prostate-specific Membrane Antigen: Diagnostics. PET Clin. 2024;19(3):351-62.

21. de Feria Cardet RE, Hofman MS, Segard T, Yim J, Williams S, Francis RJ, et al. Is Prostate-specific Membrane Antigen Positron Emission Tomography/Computed Tomography Imaging Cost-effective in Prostate Cancer: An Analysis Informed by the proPSMA Trial. Eur Urol. 2021;79(3):413-8.

22. Hicks RJ, Murphy DG, Williams SG. Seduction by Sensitivity: Reality, Illusion, or Delusion?

The Challenge of Assessing Outcomes after PSMA Imaging Selection of Patients for Treatment. J Nucl Med. 2017;58(12):1969-71.

23. Margel D, Bernstine H, Groshar D, Ber Y, Nezrit O, Segal N, et al. Diagnostic Performance of (68)Ga Prostate-specific Membrane Antigen PET/MRI Compared with Multiparametric MRI for Detecting Clinically Significant Prostate Cancer. Radiology. 2021;301(2):379-86.

24. Manfredi C, Fernández-Pascual E, Arcaniolo D, Emberton M, Sanchez-Salas R, Artigas Guix C, et al. The Role of Prostate-specific Membrane Antigen Positron Emission Tomography/Magnetic Resonance Imaging in Primary and Recurrent Prostate Cancer: A Systematic Review of the Literature. Eur Urol Focus. 2022;8(4):942-57.

25. McInnes MDF, Moher D, Thombs BD, McGrath TA, Bossuyt PM, Clifford T, et al. Preferred Reporting Items for a Systematic Review and Meta-analysis of Diagnostic Test Accuracy Studies: The PRISMA-DTA Statement. Jama. 2018;319(4):388-96.

26. Whiting PF, Rutjes AW, Westwood ME, Mallett S, Deeks JJ, Reitsma JB, et al. QUADAS-2: a revised tool for the quality assessment of diagnostic accuracy studies. Ann Intern Med. 2011;155(8):529-36.

27. Balshem H, Helfand M, Schünemann HJ, Oxman AD, Kunz R, Brozek J, et al. GRADE guidelines: 3. Rating the quality of evidence. J Clin Epidemiol. 2011;64(4):401-6.

28. Van Damme J, Tombal B, Collette L, Van Nieuwenhove S, Pasoglou V, Gérard T, et al. Comparison of (68)Ga-Prostate Specific Membrane Antigen (PSMA) Positron Emission Tomography Computed Tomography (PET-CT) and Whole-Body Magnetic Resonance Imaging (WB-MRI) with Diffusion Sequences (DWI) in the Staging of Advanced Prostate

Cancer. Cancers (Basel). 2021;13(21).

29. Çelen S, Gültekin A, Özlülerden Y, Mete A, Sağtaş E, Ufuk F, et al. Comparison of 68Ga-PSMA-I/T PET-CT and Multiparametric MRI for Locoregional Staging of Prostate Cancer Patients: A Pilot Study. Urol Int. 2020;104(9-10):684-91.

30. Yilmaz B, Turkay R, Colakoglu Y, Baytekin HF, Ergul N, Sahin S, et al. Comparison of preoperative locoregional Ga-68 PSMA-11 PET-CT and mp-MRI results with postoperative histopathology of prostate cancer. Prostate. 2019;79(9):1007-17.

31. Kalapara AA, Ballok ZE, Ramdave S, O'Sullivan R, Ryan A, Konety B, et al. Combined Utility of (68)Ga-Prostate-specific Membrane Antigen Positron Emission Tomography/Computed Tomography and Multiparametric Magnetic Resonance Imaging in Predicting Prostate Biopsy Pathology. Eur Urol Oncol. 2022;5(3):314-20.

32. Bodar YJL, Zwezerijnen B, van der Voorn PJ, Jansen BHE, Smit RS, Kol SQ, et al. Prospective analysis of clinically significant prostate cancer detection with [(18)F]DCFPyL PET/MRI compared to multiparametric MRI: a comparison with the histopathology in the radical prostatectomy specimen, the ProStaPET study. Eur J Nucl Med Mol Imaging. 2022;49(5):1731-42.

33. Parathithasan N, Perry E, Taubman K, Hegarty J, Talwar A, Wong LM, et al. Combination of MRI prostate and 18F-DCFPyl PSMA PET/CT detects all clinically significant prostate cancers in treatment-naive patients: An international multicentre retrospective study. J Med Imaging Radiat Oncol. 2022;66(7):927-35.

34. Koseoglu E, Kordan Y, Kilic M, Sal O, Seymen H, Kiremit MC, et al. Diagnostic ability of Ga-68 PSMA PET to detect dominant and non-dominant tumors, upgrading and adverse

pathology in patients with PIRADS 4-5 index lesions undergoing radical prostatectomy. Prostate Cancer Prostatic Dis. 2021;24(1):202-9.

35. Privé BM, Israël B, Schilham MGM, Muselaers CHJ, Zámecnik P, Mulders PFA, et al. Evaluating F-18-PSMA-1007-PET in primary prostate cancer and comparing it to multi-parametric MRI and histopathology. Prostate Cancer Prostatic Dis. 2021;24(2):423-30.

36. Soni BK, Verma P, Shah AK, Singh R, Sonawane S, Asopa RV. Comparison of Multiparametric Magnetic Resonance Imaging and Gallium-68 Prostate-Specific Membrane Antigen Positron Emission Tomography/Computed Tomography for Detecting Carcinoma Prostate in Patients with Serum Prostate-Specific Antigen between 4 and 20 ng/ml. Indian J Nucl Med. 2021;36(3):245-51.

37. Metser U, Ortega C, Perlis N, Lechtman E, Berlin A, Anconina R, et al. Detection of clinically significant prostate cancer with (18)F-DCFPyL PET/multiparametric MR. Eur J Nucl Med Mol Imaging. 2021;48(11):3702-11.

38. Emmett L, Buteau J, Papa N, Moon D, Thompson J, Roberts MJ, et al. The Additive Diagnostic Value of Prostate-specific Membrane Antigen Positron Emission Tomography Computed Tomography to Multiparametric Magnetic Resonance Imaging Triage in the Diagnosis of Prostate Cancer (PRIMARY): A Prospective Multicentre Study. Eur Urol. 2021;80(6):682-9.

39. Kubihal V, Sharma S, Kumar R, Seth A, Kumar R, Kaushal S, et al. Multiparametric Magnetic Resonance Imaging, (68)Ga Prostate-Specific Membrane Antigen Positron Emission Tomography-Computed Tomography, and Respective Quantitative Parameters in Detection and Localization of Clinically Significant Prostate Cancer in Intermediate- and High-Risk Group

Patients: An Indian Demographic Study. Indian J Nucl Med. 2021;36(4):362-70.

40. Chen M, Zhang Q, Zhang C, Zhou YH, Zhao X, Fu Y, et al. Comparison of (68)Ga-prostate-specific membrane antigen (PSMA) positron emission tomography/computed tomography (PET/CT) and multi-parametric magnetic resonance imaging (MRI) in the evaluation of tumor extension of primary prostate cancer. Transl Androl Urol. 2020;9(2):382-90.

41. Brauchli D, Singh D, Chabert C, Somasundaram A, Collie L. Tumour-capsule interface measured on 18F-DCFPyL PSMA positron emission tomography/CT imaging comparable to multi-parametric MRI in predicting extra-prostatic extension of prostate cancer at initial staging. J Med Imaging Radiat Oncol. 2020;64(6):829-38.

42. Li Y, Han D, Wu P, Ren J, Ma S, Zhang J, et al. Comparison of (68)Ga-PSMA-617 PET/CT with mpMRI for the detection of PCa in patients with a PSA level of 4-20 ng/ml before the initial biopsy. Sci Rep. 2020;10(1):10963.

43. Gaur S, Mena E, Harmon SA, Lindenberg ML, Adler S, Ton AT, et al. Prospective Evaluation of (18)F-DCFPyL PET/CT in Detection of High-Risk Localized Prostate Cancer: Comparison With mpMRI. AJR Am J Roentgenol. 2020;215(3):652-9.

44. Wang L, Yu F, Yang L, Zang S, Xue H, Yin X, et al. 68Ga-PSMA-11 PET/CT combining ADC value of MRI in the diagnosis of naive prostate cancer: Perspective of radiologist. Medicine (Baltimore). 2020;99(36):e20755.

45. Muehlematter UJ, Burger IA, Becker AS, Schawkat K, Hötker AM, Reiner CS, et al. Diagnostic Accuracy of Multiparametric MRI versus (68)Ga-PSMA-11 PET/MRI for Extracapsular Extension and Seminal Vesicle Invasion in Patients with Prostate Cancer.

Radiology. 2019;293(2):350-8.

46. van Leeuwen PJ, Donswijk M, Nandurkar R, Stricker P, Ho B, Heijmink S, et al. Gallium-68-prostate-specific membrane antigen ((68) Ga-PSMA) positron emission tomography (PET)/computed tomography (CT) predicts complete biochemical response from radical prostatectomy and lymph node dissection in intermediate- and high-risk prostate cancer. BJU Int. 2019;124(1):62-8.

47. Kumar N, Yadav S, Kumar S, Saurav K, Prasad V, Vasudeva P. Comparison of percentage free PSA, MRI and GaPSMA PET scan for diagnosing cancer prostate in men with PSA between 4 and 20 ng/ml. Indian J Urol. 2019;35(3):202-7.

48. Scheltema MJ, Chang JI, Stricker PD, van Leeuwen PJ, Nguyen QA, Ho B, et al. Diagnostic accuracy of (68) Ga-prostate-specific membrane antigen (PSMA) positron-emission tomography (PET) and multiparametric (mp)MRI to detect intermediate-grade intra-prostatic prostate cancer using whole-mount pathology: impact of the addition of (68) Ga-PSMA PET to mpMRI. BJU Int. 2019;124 Suppl 1:42-9.

49. Chen M, Zhang Q, Zhang C, Zhao X, Marra G, Gao J, et al. Combination of (68)Ga-PSMA PET/CT and Multiparametric MRI Improves the Detection of Clinically Significant Prostate Cancer: A Lesion-by-Lesion Analysis. J Nucl Med. 2019;60(7):944-9.

50. Berger I, Annabattula C, Lewis J, Shetty DV, Kam J, Maclean F, et al. (68)Ga-PSMA PET/CT vs. mpMRI for locoregional prostate cancer staging: correlation with final histopathology. Prostate Cancer Prostatic Dis. 2018;21(2):204-11.

51. Hicks RM, Simko JP, Westphalen AC, Nguyen HG, Greene KL, Zhang L, et al. Diagnostic Accuracy of (68)Ga-PSMA-11 PET/MRI Compared with Multiparametric MRI in the Detection

of Prostate Cancer. Radiology. 2018;289(3):730-7.

52. Park SY, Zacharias C, Harrison C, Fan RE, Kunder C, Hatami N, et al. Gallium 68 PSMA-11 PET/MR Imaging in Patients with Intermediate- or High-Risk Prostate Cancer. Radiology. 2018;288(2):495-505.

53. Jena A, Taneja R, Taneja S, Singh A, Kumar V, Agarwal A, et al. Improving Diagnosis of Primary Prostate Cancer With Combined (68)Ga-Prostate-Specific Membrane Antigen-HBED-CC Simultaneous PET and Multiparametric MRI and Clinical Parameters. AJR Am J Roentgenol. 2018;211(6):1246-53.

54. Al-Bayati M, Grueneisen J, Lütje S, Sawicki LM, Suntharalingam S, Tschirdewahn S, et al. Integrated 68Gallium Labelled Prostate-Specific Membrane Antigen-11 Positron Emission Tomography/Magnetic Resonance Imaging Enhances Discriminatory Power of Multi-Parametric Prostate Magnetic Resonance Imaging. Urol Int. 2018;100(2):164-71.

55. Turkbey B, Mena E, Lindenberg L, Adler S, Bednarova S, Berman R, et al. 18F-DCFBC Prostate-Specific Membrane Antigen-Targeted PET/CT Imaging in Localized Prostate Cancer: Correlation With Multiparametric MRI and Histopathology. Clin Nucl Med. 2017;42(10):735-40.

56. Eiber M, Weirich G, Holzapfel K, Souvatzoglou M, Haller B, Rauscher I, et al. Simultaneous (68)Ga-PSMA HBED-CC PET/MRI Improves the Localization of Primary Prostate Cancer. Eur Urol. 2016;70(5):829-36.

57. Rowe SP, Gage KL, Faraj SF, Macura KJ, Cornish TC, Gonzalez-Roibon N, et al. ^{18}F-DCFBC PET/CT for PSMA-Based Detection and Characterization of Primary Prostate Cancer. J Nucl Med. 2015;56(7):1003-10.

58. Pallavi UN, Gogoi S, Thakral P, Malasani V, Sharma K, Manda D, et al. Incremental

Value of Ga-68 Prostate-Specific Membrane Antigen-11 Positron-Emission Tomography/Computed Tomography Scan for Preoperative Risk Stratification of Prostate Cancer. Indian J Nucl Med. 2020;35(2):93-9.

59. Arslan A, Karaarslan E, Güner AL, Sağlıcan Y, Tuna MB, Kural AR. Comparing the Diagnostic Performance of Multiparametric Prostate MRI Versus 68Ga-PSMA PET-CT in the Evaluation Lymph Node Involvement and Extraprostatic Extension. Acad Radiol. 2022;29(5):698-704.

60. Patel KS, Singh T, Raghuvanshi K, Sonar S, Chaudhari R. A comparison study of 68gallium-prostate-specific membrane antigen positron emission tomography-computed tomography and multiparametric magnetic resonance imaging for locoregional staging of prostate cancer. Urol Sci. 2024;35(1):36-41.

61. Wang G, Li L, Zang J, Hong H, Zhu L, Kung HF, et al. Head-to-Head Comparison of 68 Ga-P16-093 and 68 Ga-PSMA-617 PET/CT in Patients With Primary Prostate Cancer : A Pilot Study. Clin Nucl Med. 2023;48(4):289-95.

62. Ghaedian T, Abdinejad M, Nasrollahi H, Ghaedian M, Firuzyar T. Comparing the role of 99m Tc-HYNIC-PSMA-11 and 99m Tc-MDP scintigraphy for the initial staging of intermediate to high-risk prostate cancer. Nucl Med Commun. 2023;44(10):864-9.

63. Beheshti M, Taimen P, Kemppainen J, Jambor I, Müller A, Loidl W, et al. Value of (68)Ga-labeled bombesin antagonist (RM2) in the detection of primary prostate cancer comparing with [(18)F]fluoromethylcholine PET-CT and multiparametric MRI-a phase I/II study. Eur Radiol. 2023;33(1):472-82.

64. Zhang Y, Shi Y, Ye L, Li T, Wei Y, Lin Z, et al. Improving diagnostic efficacy of primary

prostate cancer with combined (99m)Tc-PSMA SPECT/CT and multiparametric-MRI and quantitative parameters. Front Oncol. 2023;13:1193370.

65. Skawran SM, Sanchez V, Ghafoor S, Hötker AM, Burger IA, Huellner MW, et al. Primary staging in patients with intermediate- and high-risk prostate cancer: Multiparametric MRI and (68)Ga-PSMA-PET/MRI - What is the value of quantitative data from multiparametric MRI alone or in conjunction with clinical information? Eur J Radiol. 2022;146:110044.

66. Szigeti F, Schweighofer-Zwink G, Meissnitzer M, Hauser-Kronberger C, Hitzl W, Kunit T, et al. Incremental Impact of [(68) Ga]Ga-PSMA-11 PET/CT in Primary N and M Staging of Prostate Cancer Prior to Curative-Intent Surgery: a Prospective Clinical Trial in Comparison with mpMRI. Mol Imaging Biol. 2022;24(1):50-9.

67. Kulkarni SC, Sundaram PS, Padma S. In primary lymph nodal staging of patients with high-risk and intermediate-risk prostate cancer, how critical is the role of Gallium-68 prostate-specific membrane antigen positron emission tomography-computed tomography? Nucl Med Commun. 2020;41(2):139-46.

68. Frumer M, Milk N, Rinott Mizrahi G, Bistritzky S, Sternberg I, Leibovitch I, et al. A comparison between (68)Ga-labeled prostate-specific membrane antigen-PET/CT and multiparametric MRI for excluding regional metastases prior to radical prostatectomy. Abdom Radiol (NY). 2020;45(12):4194-201.

69. Franklin A, Yaxley WJ, Raveenthiran S, Coughlin G, Gianduzzo T, Kua B, et al. Histological comparison between predictive value of preoperative 3-T multiparametric MRI and (68) Ga-PSMA PET/CT scan for pathological outcomes at radical prostatectomy and pelvic lymph node dissection for prostate cancer. BJU Int. 2021;127(1):71-9.

70. Gupta M, Choudhury PS, Hazarika D, Rawal S. A Comparative Study of (68)Gallium-Prostate Specific Membrane Antigen Positron Emission Tomography-Computed Tomography and Magnetic Resonance Imaging for Lymph Node Staging in High Risk Prostate Cancer Patients: An Initial Experience. World J Nucl Med. 2017;16(3):186-91.

71. Zhang Q, Zang S, Zhang C, Fu Y, Lv X, Zhang Q, et al. Comparison of (68)Ga-PSMA-11 PET-CT with mpMRI for preoperative lymph node staging in patients with intermediate to high-risk prostate cancer. J Transl Med. 2017;15(1):230.

72. Kaufmann S, Kruck S, Gatidis S, Hepp T, Thaiss WM, Hennenlotter J, et al. Simultaneous whole-body PET/MRI with integrated multiparametric MRI for primary staging of high-risk prostate cancer. World J Urol. 2020;38(10):2513-21.

73. Lecouvet FE, El Mouedden J, Collette L, Coche E, Danse E, Jamar F, et al. Can whole-body magnetic resonance imaging with diffusion-weighted imaging replace Tc 99m bone scanning and computed tomography for single-step detection of metastases in patients with high-risk prostate cancer? Eur Urol. 2012;62(1):68-75.

74. Kroenke M, Wurzer A, Schwamborn K, Ulbrich L, Jooß L, Maurer T, et al. Histologically Confirmed Diagnostic Efficacy of (18)F-rhPSMA-7 PET for N-Staging of Patients with Primary High-Risk Prostate Cancer. J Nucl Med. 2020;61(5):710-5.

75. Malaspina S, Anttinen M, Taimen P, Jambor I, Sandell M, Rinta-Kiikka I, et al. Prospective comparison of (18)F-PSMA-1007 PET/CT, whole-body MRI and CT in primary nodal staging of unfavourable intermediate- and high-risk prostate cancer. Eur J Nucl Med Mol Imaging. 2021;48(9):2951-9.

76. Maurer T, Gschwend JE, Rauscher I, Souvatzoglou M, Haller B, Weirich G, et al.

Diagnostic Efficacy of (68)Gallium-PSMA Positron Emission Tomography Compared to Conventional Imaging for Lymph Node Staging of 130 Consecutive Patients with Intermediate to High Risk Prostate Cancer. J Urol. 2016;195(5):1436-43.

77. Öbek C, Doğanca T, Demirci E, Ocak M, Kural AR, Yıldırım A, et al. The accuracy of (68)Ga-PSMA PET/CT in primary lymph node staging in high-risk prostate cancer. Eur J Nucl Med Mol Imaging. 2017;44(11):1806-12.

78. Petersen LJ, Nielsen JB, Langkilde NC, Petersen A, Afshar-Oromieh A, De Souza NM, et al. (68)Ga-PSMA PET/CT compared with MRI/CT and diffusion-weighted MRI for primary lymph node staging prior to definitive radiotherapy in prostate cancer: a prospective diagnostic test accuracy study. World J Urol. 2020;38(4):939-48.

79. Pienta KJ, Gorin MA, Rowe SP, Carroll PR, Pouliot F, Probst S, et al. A Phase 2/3 Prospective Multicenter Study of the Diagnostic Accuracy of Prostate Specific Membrane Antigen PET/CT with (18)F-DCFPyL in Prostate Cancer Patients (OSPREY). J Urol. 2021;206(1):52-61.

80. Qiao Z, Wang S, Wang H, He B, Shi Z, Zhou H, et al. Diagnostic capability of 18F-PSMA PET-MRI and pelvic MRI plus bone scan in treatment-naive prostate cancer: a single-center paired validating confirmatory study. Int J Surg. 2024;110(1):87-94.

81. Venkitaraman R, Cook GJ, Dearnaley DP, Parker CC, Huddart RA, Khoo V, et al. Does magnetic resonance imaging of the spine have a role in the staging of prostate cancer? Clin Oncol (R Coll Radiol). 2009;21(1):39-42.

82. Giovanella L, Castellani M, Suriano S, Ruberto T, Ceriani L, Tagliabue L, et al. Multi-field-of-view SPECT is superior to whole-body scanning for assessing metastatic bone

disease in patients with prostate cancer. Tumori. 2011;97(5):629-33.

83. Picchio M, Spinapolice EG, Fallanca F, Crivellaro C, Giovacchini G, Gianolli L, et al. [11C]Choline PET/CT detection of bone metastases in patients with PSA progression after primary treatment for prostate cancer: comparison with bone scintigraphy. Eur J Nucl Med Mol Imaging. 2012;39(1):13-26.

84. Kitajima K, Murphy RC, Nathan MA, Froemming AT, Hagen CE, Takahashi N, et al. Detection of recurrent prostate cancer after radical prostatectomy: comparison of 11C-choline PET/CT with pelvic multiparametric MR imaging with endorectal coil. J Nucl Med. 2014;55(2):223-32.

85. Takesh M, Odat Allh K, Adams S, Zechmann C. Diagnostic Role of (18)F-FECH-PET/CT Compared with Bone Scan in Evaluating the Prostate Cancer Patients Referring with Biochemical Recurrence. ISRN Oncol. 2012;2012:815234.

86. Fonager RF, Zacho HD, Langkilde NC, Fledelius J, Ejlersen JA, Haarmark C, et al. Diagnostic test accuracy study of (18)F-sodium fluoride PET/CT, (99m)Tc-labelled diphosphonate SPECT/CT, and planar bone scintigraphy for diagnosis of bone metastases in newly diagnosed, high-risk prostate cancer. Am J Nucl Med Mol Imaging. 2017;7(5):218-27.

87. Huysse W, Lecouvet F, Castellucci P, Ost P, Lambrecht V, Artigas C, et al. Prospective Comparison of F-18 Choline PET/CT Scan Versus Axial MRI for Detecting Bone Metastasis in Biochemically Relapsed Prostate Cancer Patients. Diagnostics (Basel). 2017;7(4).

88. Lengana T, Lawal IO, Boshomane TG, Popoola GO, Mokoala KMG, Moshokoa E, et al. (68)Ga-PSMA PET/CT Replacing Bone Scan in the Initial Staging of Skeletal Metastasis in Prostate Cancer: A Fait Accompli? Clin Genitourin Cancer. 2018;16(5):392-401.

89. Kitajima K, Fukushima K, Yamamoto S, Kato T, Odawara S, Takaki H, et al. Diagnostic performance of (11)C-choline PET/CT and bone scintigraphy in the detection of bone metastases in patients with prostate cancer. Nagoya J Med Sci. 2017;79(3):387-99.

90. Dyrberg E, Hendel HW, Huynh THV, Klausen TW, Løgager VB, Madsen C, et al. (68)Ga-PSMA-PET/CT in comparison with (18)F-fluoride-PET/CT and whole-body MRI for the detection of bone metastases in patients with prostate cancer: a prospective diagnostic accuracy study. Eur Radiol. 2019;29(3):1221-30.

91. Simsek DH, Sanli Y, Civan C, Engin MN, Isik EG, Ozkan ZG, et al. Does bone scintigraphy still have a role in the era of 68 Ga-PSMA PET/CT in prostate cancer? Ann Nucl Med. 2020;34(7):476-85.

92. Zacho HD, Ravn S, Afshar-Oromieh A, Fledelius J, Ejlersen JA, Petersen LJ. Added value of (68)Ga-PSMA PET/CT for the detection of bone metastases in patients with newly diagnosed prostate cancer and a previous (99m)Tc bone scintigraphy. EJNMMI Res. 2020;10(1):31.

93. Pyka T, Okamoto S, Dahlbender M, Tauber R, Retz M, Heck M, et al. Comparison of bone scintigraphy and (68)Ga-PSMA PET for skeletal staging in prostate cancer. Eur J Nucl Med Mol Imaging. 2016;43(12):2114-21.

94. Uslu-Beşli L, Sağer S, Akgün E, Asa S, Şahin OE, Demirdağ Ç, et al. Comparison of Ga-68 PSMA positron emission tomography/computerized tomography with Tc-99m MDP bone scan in prostate cancer patients. Turk J Med Sci. 2019;49(1):301-10.

95. Caglar M, Tuncel M, Yildiz E, Karabulut E. Bone scintigraphy as a gatekeeper for the detection of bone metastases in patients with prostate cancer: comparison with Ga-68 PSMA

PET/CT. Ann Nucl Med. 2020;34(12):932-41.

96. Mosavi F, Johansson S, Sandberg DT, Turesson I, Sörensen J, Ahlström H. Whole-body diffusion-weighted MRI compared with (18)F-NaF PET/CT for detection of bone metastases in patients with high-risk prostate carcinoma. AJR Am J Roentgenol. 2012;199(5):1114-20.

97. Mortensen MA, Poulsen MH, Gerke O, Jakobsen JS, Høilund-Carlsen PF, Lund L. (18)F-Fluoromethylcholine-positron emission tomography/computed tomography for diagnosing bone and lymph node metastases in patients with intermediate- or high-risk prostate cancer. Prostate Int. 2019;7(3):119-23.

98. de Leiris N, Leenhardt J, Boussat B, Montemagno C, Seiller A, Phan Sy O, et al. Does whole-body bone SPECT/CT provide additional diagnostic information over [18F]-FCH PET/CT for the detection of bone metastases in the setting of prostate cancer biochemical recurrence? Cancer Imaging. 2020;20(1):58.

99. Zacho HD, Nielsen JB, Afshar-Oromieh A, Haberkorn U, deSouza N, De Paepe K, et al. Prospective comparison of (68)Ga-PSMA PET/CT, (18)F-sodium fluoride PET/CT and diffusion weighted-MRI at for the detection of bone metastases in biochemically recurrent prostate cancer. Eur J Nucl Med Mol Imaging. 2018;45(11):1884-97.

100. Fuccio C, Castellucci P, Schiavina R, Santi I, Allegri V, Pettinato V, et al. Role of 11C-choline PET/CT in the restaging of prostate cancer patients showing a single lesion on bone scintigraphy. Ann Nucl Med. 2010;24(6):485-92.

101. Poulsen MH, Petersen H, Høilund-Carlsen PF, Jakobsen JS, Gerke O, Karstoft J, et al. Spine metastases in prostate cancer: comparison of technetium-99m-MDP whole-body bone scintigraphy, [(18) F]choline positron emission tomography(PET)/computed tomography (CT)

and [(18) F]NaF PET/CT. BJU Int. 2014;114(6):818-23.

102. Wieder H, Beer AJ, Holzapfel K, Henninger M, Maurer T, Schwarzenboeck S, et al. 11C-choline PET/CT and whole-body MRI including diffusion-weighted imaging for patients with recurrent prostate cancer. Oncotarget. 2017;8(39):66516-27.

103. Garcia JR, Moreno C, Valls E, Cozar P, Bassa P, Soler M, et al. [Diagnostic performance of bone scintigraphy and (11)C-Choline PET/CT in the detection of bone metastases in patients with biochemical recurrence of prostate cancer]. Rev Esp Med Nucl Imagen Mol. 2015;34(3):155-61.

104. Even-Sapir E, Metser U, Mishani E, Lievshitz G, Lerman H, Leibovitch I. The detection of bone metastases in patients with high-risk prostate cancer: 99mTc-MDP Planar bone scintigraphy, single- and multi-field-of-view SPECT, 18F-fluoride PET, and 18F-fluoride PET/CT. J Nucl Med. 2006;47(2):287-97.

105. Nozaki T, Yasuda K, Akashi T, Fuse H. Usefulness of single photon emission computed tomography imaging in the detection of lumbar vertebral metastases from prostate cancer. Int J Urol. 2008;15(6):516-9.

106. Lecouvet FE, Geukens D, Stainier A, Jamar F, Jamart J, d'Othée BJ, et al. Magnetic resonance imaging of the axial skeleton for detecting bone metastases in patients with high-risk prostate cancer: diagnostic and cost-effectiveness and comparison with current detection strategies. J Clin Oncol. 2007;25(22):3281-7.

107. Saule L, Radzina M, Liepa M, Roznere L, Kalnina M, Lioznovs A, et al. Diagnostic scope of (18)F-PSMA-1007 PET/CT: comparison with multiparametric MRI and bone scintigraphy for the assessment of early prostate cancer recurrence. Am J Nucl Med Mol Imaging.

2021;11(5):395-405.

108. Radzina M, Tirane M, Roznere L, Zemniece L, Dronka L, Kalnina M, et al. Accuracy of (68)Ga-PSMA-11 PET/CT and multiparametric MRI for the detection of local tumor and lymph node metastases in early biochemical recurrence of prostate cancer. Am J Nucl Med Mol Imaging. 2020;10(2):106-18.

109. Tseng JR, Yu KJ, Liu FY, Yang LY, Hong JH, Yen TC, et al. Comparison between (68)Ga-PSMA-11 PET/CT and multiparametric magnetic resonance imaging in patients with biochemically recurrent prostate cancer following robot-assisted radical prostatectomy. J Formos Med Assoc. 2021;120(1 Pt 3):688-96.

110. Nanni C, Zanoni L, Pultrone C, Schiavina R, Brunocilla E, Lodi F, et al. (18)F-FACBC (anti1-amino-3-(18)F-fluorocyclobutane-1-carboxylic acid) versus (11)C-choline PET/CT in prostate cancer relapse: results of a prospective trial. Eur J Nucl Med Mol Imaging. 2016;43(9):1601-10.

111. Wilson ZJ, Xu G, Tewari SO, Lu Y. Comparison of PSMA-based (18)F-DCFPyL PET/CT and Tc-99m MDP bone scan in detection of bone metastasis in prostate cancer. Am J Nucl Med Mol Imaging. 2023;13(1):1-10.

112. Jannusch K, Bruckmann NM, Morawitz J, Boschheidgen M, Quick HH, Hermann K, et al. Recurrent prostate cancer: combined role for MRI and PSMA-PET in (68)Ga-PSMA-11 PET/MRI. Eur Radiol. 2024;34(7):4789-800.

113. Hu X, Cao Y, Ji B, Zhao M, Wen Q, Chen B. Comparative study of (18)F-DCFPyL PET/CT and (99m)Tc-MDP SPECT/CT bone imaging for the detection of bone metastases in prostate cancer. Front Med (Lausanne). 2023;10:1201977.

114. Asa S, Ozgur E, Uslu-Besli L, Ince B, Sager S, Demirdag C, et al. Hybrid Ga-68 prostate-specific membrane antigen PET/MRI in the detection of skeletal metastasis in patients with newly diagnosed prostate cancer: Contribution of each part to the diagnostic performance. Nucl Med Commun. 2023;44(1):65-73.

115. Zhang Y, Lin Z, Li T, Wei Y, Yu M, Ye L, et al. Head-to-head comparison of (99m)Tc-PSMA and (99m)Tc-MDP SPECT/CT in diagnosing prostate cancer bone metastasis: a prospective, comparative imaging trial. Sci Rep. 2022;12(1):15993.

116. Kabunda J, Gabela L, Kalinda C, Aldous C, Pillay V, Nyakale N. Comparing 99mTc-PSMA to 99mTc-MDP in Prostate Cancer Staging of the Skeletal System. Clin Nucl Med. 2021;46(7):562-8.

117. Chen B, Wei P, Macapinlac HA, Lu Y. Comparison of 18F-Fluciclovine PET/CT and 99mTc-MDP bone scan in detection of bone metastasis in prostate cancer. Nucl Med Commun. 2019;40(9):940-6.

118. Wu J, Lu AD, Zhang LP, Zuo YX, Jia YP. [Study of clinical outcome and prognosis in pediatric core binding factor-acute myeloid leukemia]. Zhonghua Xue Ye Xue Za Zhi. 2019;40(1):52-7.

119. Jadvar H, Desai B, Ji L, Conti PS, Dorff TB, Groshen SG, et al. Prospective evaluation of 18F-NaF and 18F-FDG PET/CT in detection of occult metastatic disease in biochemical recurrence of prostate cancer. Clin Nucl Med. 2012;37(7):637-43.

120. Afshar-Oromieh A, Zechmann CM, Malcher A, Eder M, Eisenhut M, Linhart HG, et al. Comparison of PET imaging with a (68)Ga-labelled PSMA ligand and (18)F-choline-based PET/CT for the diagnosis of recurrent prostate cancer. Eur J Nucl Med Mol Imaging.

2014;41(1):11-20.

121. Piccardo A, Paparo F, Piccazzo R, Naseri M, Ricci P, Marziano A, et al. Value of fused 18F-Choline-PET/MRI to evaluate prostate cancer relapse in patients showing biochemical recurrence after EBRT: preliminary results. Biomed Res Int. 2014;2014:103718.

122. Dietlein M, Kobe C, Kuhnert G, Stockter S, Fischer T, Schomäcker K, et al. Comparison of [(18)F]DCFPyL and [(68)Ga]Ga-PSMA-HBED-CC for PSMA-PET Imaging in Patients with Relapsed Prostate Cancer. Mol Imaging Biol. 2015;17(4):575-84.

123. Morigi JJ, Stricker PD, van Leeuwen PJ, Tang R, Ho B, Nguyen Q, et al. Prospective Comparison of 18F-Fluoromethylcholine Versus 68Ga-PSMA PET/CT in Prostate Cancer Patients Who Have Rising PSA After Curative Treatment and Are Being Considered for Targeted Therapy. J Nucl Med. 2015;56(8):1185-90.

124. Nanni C, Schiavina R, Brunocilla E, Boschi S, Borghesi M, Zanoni L, et al. 18F-Fluciclovine PET/CT for the Detection of Prostate Cancer Relapse: A Comparison to 11C-Choline PET/CT. Clin Nucl Med. 2015;40(8):e386-91.

125. Odewole OA, Tade FI, Nieh PT, Savir-Baruch B, Jani AB, Master VA, et al. Recurrent prostate cancer detection with anti-3-[(18)F]FACBC PET/CT: comparison with CT. Eur J Nucl Med Mol Imaging. 2016;43(10):1773-83.

126. Lütje S, Cohnen J, Gomez B, Grüneisen J, Sawicki L, Rübben H, et al. Integrated (68)Ga-HBED-CC-PSMA-PET/MRI in patients with suspected recurrent prostate cancer. Nuklearmedizin. 2017;56(3):73-81.

127. Schwenck J, Rempp H, Reischl G, Kruck S, Stenzl A, Nikolaou K, et al. Comparison of (68)Ga-labelled PSMA-11 and (11)C-choline in the detection of prostate cancer metastases by

PET/CT. Eur J Nucl Med Mol Imaging. 2017;44(1):92-101.

128. Cantiello F, Crocerossa F, Russo GI, Gangemi V, Ferro M, Vartolomei MD, et al. Comparison Between (64)Cu-PSMA-617 PET/CT and (18)F-Choline PET/CT Imaging in Early Diagnosis of Prostate Cancer Biochemical Recurrence. Clin Genitourin Cancer. 2018;16(5):385-91.

129. Calais J, Ceci F, Eiber M, Hope TA, Hofman MS, Rischpler C, et al. (18)F-fluciclovine PET-CT and (68)Ga-PSMA-11 PET-CT in patients with early biochemical recurrence after prostatectomy: a prospective, single-centre, single-arm, comparative imaging trial. Lancet Oncol. 2019;20(9):1286-94.

130. Pernthaler B, Kulnik R, Gstettner C, Salamon S, Aigner RM, Kvaternik H. A Prospective Head-to-Head Comparison of 18F-Fluciclovine With 68Ga-PSMA-11 in Biochemical Recurrence of Prostate Cancer in PET/CT. Clin Nucl Med. 2019;44(10):e566-e73.

131. Sawicki LM, Kirchner J, Buddensieck C, Antke C, Ullrich T, Schimmöller L, et al. Prospective comparison of whole-body MRI and (68)Ga-PSMA PET/CT for the detection of biochemical recurrence of prostate cancer after radical prostatectomy. Eur J Nucl Med Mol Imaging. 2019;46(7):1542-50.

132. Witkowska-Patena E, Giżewska A, Dziuk M, Miśko J, Budzyńska A, Walęcka-Mazur A. Head-to-Head Comparison of 18F-Prostate-Specific Membrane Antigen-1007 and 18F-Fluorocholine PET/CT in Biochemically Relapsed Prostate Cancer. Clin Nucl Med. 2019;44(12):e629-e33.

133. Joshi A, Roberts MJ, Perera M, Williams E, Rhee H, Pryor D, et al. The clinical efficacy of PSMA PET/MRI in biochemically recurrent prostate cancer compared with standard of care

imaging modalities and confirmatory histopathology: results of a single-centre, prospective clinical trial. Clin Exp Metastasis. 2020;37(4):551-60.

134. Lindenberg L, Mena E, Turkbey B, Shih JH, Reese SE, Harmon SA, et al. Evaluating Biochemically Recurrent Prostate Cancer: Histologic Validation of (18)F-DCFPyL PET/CT with Comparison to Multiparametric MRI. Radiology. 2020;296(3):564-72.

135. Paparo F, Peirano A, Matos J, Bacigalupo L, Rossi U, Mussetto I, et al. Diagnostic value of retrospectively fused (64)CuCl(2) PET/MRI in biochemical relapse of prostate cancer: comparison with fused (18)F-Choline PET/MRI, (64)CuCl2 PET/CT, (18)F-Choline PET/CT, and mpMRI. Abdom Radiol (NY). 2020;45(11):3896-906.

136. Regula N, Kostaras V, Johansson S, Trampal C, Lindström E, Lubberink M, et al. Comparison of (68)Ga-PSMA-11 PET/CT with (11)C-acetate PET/CT in re-staging of prostate cancer relapse. Sci Rep. 2020;10(1):4993.

137. Baratto L, Song H, Duan H, Hatami N, Bagshaw HP, Buyyounouski M, et al. PSMA- and GRPR-Targeted PET: Results from 50 Patients with Biochemically Recurrent Prostate Cancer. J Nucl Med. 2021;62(11):1545-9.

138. Evangelista L, Cassarino G, Lauro A, Morlacco A, Sepulcri M, Nguyen AAL, et al. Comparison of MRI, PET, and 18F-choline PET/MRI in patients with oligometastatic recurrent prostate cancer. Abdom Radiol (NY). 2021;46(9):4401-9.

139. Jentjens S, Mai C, Ahmadi Bidakhvidi N, De Coster L, Mertens N, Koole M, et al. Prospective comparison of simultaneous [(68)Ga]Ga-PSMA-11 PET/MR versus PET/CT in patients with biochemically recurrent prostate cancer. Eur Radiol. 2022;32(2):901-11.

140. Lengana T, Lawal IO, Rensburg CV, Mokoala KMG, Moshokoa E, Ridgard T, et al. A

comparison of the diagnostic performance of (18)F-PSMA-1007 and (68)GA-PSMA-11 in the same patients presenting with early biochemical recurrence. Hell J Nucl Med. 2021;24(3):178-85.

141. Glemser PA, Rotkopf LT, Ziener CH, Beuthien-Baumann B, Weru V, Kopp-Schneider A, et al. Hybrid imaging with [(68)Ga]PSMA-11 PET-CT and PET-MRI in biochemically recurrent prostate cancer. Cancer Imaging. 2022;22(1):53.

142. Martinez J, Subramanian K, Margolis D, O'Dwyer E, Osborne J, Jhanwar Y, et al. 68Ga-PSMA-HBED-CC PET/MRI is superior to multiparametric magnetic resonance imaging in men with biochemical recurrent prostate cancer: A prospective single-institutional study. Transl Oncol. 2022;15(1):101242.

143. García-Zoghby L, Lucas-Lucas C, Amo-Salas M, Soriano-Castrejón Á M, García-Vicente AM. Head-to-Head Comparison of [(18)F]F-choline and Imaging of Prostate-Specific Membrane Antigen, Using [(18)F]DCFPyL PET/CT, in Patients with Biochemical Recurrence of Prostate Cancer. Curr Oncol. 2023;30(7):6271-88.

144. Oprea-Lager DE, Gontier E, García-Cañamaque L, Gauthé M, Olivier P, Mitjavila M, et al. [(18)F]DCFPyL PET/CT versus [(18)F]fluoromethylcholine PET/CT in Biochemical Recurrence of Prostate Cancer (PYTHON): a prospective, open label, cross-over, comparative study. Eur J Nucl Med Mol Imaging. 2023;50(11):3439-51.

145. Duan H, Moradi F, Davidzon GA, Liang T, Song H, Loening AM, et al. (68)Ga-RM2 PET-MRI versus MRI alone for evaluation of patients with biochemical recurrence of prostate cancer: a single-centre, single-arm, phase 2/3 imaging trial. Lancet Oncol. 2024;25(4):501-8.

146. Ghezzo S, Mapelli P, Samanes Gajate AM, Palmisano A, Cucchiara V, Brembilla G, et al.

Diagnostic accuracy of fully hybrid [(68)Ga]Ga-PSMA-11 PET/MRI and [(68)Ga]Ga-RM2 PET/MRI in patients with biochemically recurrent prostate cancer: a prospective single-center phase II clinical trial. Eur J Nucl Med Mol Imaging. 2024;51(3):907-18.

147. Duan H, Song H, Davidzon GA, Moradi F, Liang T, Loening A, et al. Prospective Comparison of (68)Ga-NeoB and (68)Ga-PSMA-R2 PET/MRI in Patients with Biochemically Recurrent Prostate Cancer. J Nucl Med. 2024;65(6):897-903.

148. Kim J, Lee S, Kim D, Kim HJ, Oh KT, Kim SJ, et al. Combination of [(18)F]FDG and [(18)F]PSMA-1007 PET/CT predicts tumour aggressiveness at staging and biochemical failure postoperatively in patients with prostate cancer. Eur J Nucl Med Mol Imaging. 2024;51(6):1763-72.

149. Xu L, Chen R, Yu X, Liu J, Wang Y. (18)F-FDG PET Is Not Inferior to (68)Ga-PSMA PET for Detecting Biochemical Recurrent Prostate Cancer with a High Gleason Score: A Head-to-Head Comparison Study. Diagnostics (Basel). 2023;14(1).

150. Hull GW, Rabbani F, Abbas F, Wheeler TM, Kattan MW, Scardino PT. Cancer control with radical prostatectomy alone in 1,000 consecutive patients. J Urol. 2002;167(2 Pt 1):528-34.

151. Williams IS, McVey A, Perera S, O'Brien JS, Kostos L, Chen K, et al. Modern paradigms for prostate cancer detection and management. Med J Aust. 2022;217(8):424-33.

152. Lawal IO, Ndlovu H, Kgatle M, Mokoala KMG, Sathekge MM. Prognostic Value of PSMA PET/CT in Prostate Cancer. Semin Nucl Med. 2024;54(1):46-59.

153. Ong XRS, Bagguley D, Yaxley JW, Azad AA, Murphy DG, Lawrentschuk N. Understanding the diagnosis of prostate cancer. Med J Aust. 2020;213(9):424-9.

154. Rasul S, Haug AR. Clinical Applications of PSMA PET Examination in Patients with Prostate Cancer. Cancers (Basel). 2022;14(15).

155. Li M, Zelchan R, Orlova A. The Performance of FDA-Approved PET Imaging Agents in the Detection of Prostate Cancer. Biomedicines. 2022;10(10).

156. Kaittanis C, Andreou C, Hieronymus H, Mao N, Foss CA, Eiber M, et al. Prostate-specific membrane antigen cleavage of vitamin B9 stimulates oncogenic signaling through metabotropic glutamate receptors. J Exp Med. 2018;215(1):159-75.

157. Bieth M, Krönke M, Tauber R, Dahlbender M, Retz M, Nekolla SG, et al. Exploring New Multimodal Quantitative Imaging Indices for the Assessment of Osseous Tumor Burden in Prostate Cancer Using (68)Ga-PSMA PET/CT. J Nucl Med. 2017;58(10):1632-7.

158. Eiber M, Herrmann K, Calais J, Hadaschik B, Giesel FL, Hartenbach M, et al. Prostate Cancer Molecular Imaging Standardized Evaluation (PROMISE): Proposed miTNM Classification for the Interpretation of PSMA-Ligand PET/CT. J Nucl Med. 2018;59(3):469-78.

159. Van de Wiele C, Sathekge M, de Spiegeleer B, De Jonghe PJ, Debruyne PR, Borms M, et al. PSMA expression on neovasculature of solid tumors. Histol Histopathol. 2020;35(9):919-27.

160. Lindenberg L, Ahlman M, Turkbey B, Mena E, Choyke P. Advancement of MR and PET/MR in Prostate Cancer. Semin Nucl Med. 2016;46(6):536-43.

161. Krilaviciute A, Becker N, Lakes J, Radtke JP, Kuczyk M, Peters I, et al. Digital Rectal Examination Is Not a Useful Screening Test for Prostate Cancer. Eur Urol Oncol. 2023;6(6):566-73.

162. Cornford P, van den Bergh RCN, Briers E, Van den Broeck T, Brunckhorst O, Darraugh J,

et al. EAU-EANM-ESTRO-ESUR-ISUP-SIOG Guidelines on Prostate Cancer-2024 Update. Part I: Screening, Diagnosis, and Local Treatment with Curative Intent. Eur Urol. 2024;86(2):148-63.

163. Sherafatmandjoo H, Safaei AA, Ghaderi F, Allameh F. Prostate cancer diagnosis based on multi-parametric MRI, clinical and pathological factors using deep learning. Sci Rep. 2024;14(1):14951.

164. Mohseninia N, Zamani-Siahkali N, Harsini S, Divband G, Pirich C, Beheshti M. Bone Metastasis in Prostate Cancer: Bone Scan Versus PET Imaging. Semin Nucl Med. 2024;54(1):97-118.

165. Zhou J, Gou Z, Wu R, Yuan Y, Yu G, Zhao Y. Comparison of PSMA-PET/CT, choline-PET/CT, NaF-PET/CT, MRI, and bone scintigraphy in the diagnosis of bone metastases in patients with prostate cancer: a systematic review and meta-analysis. Skeletal Radiol. 2019;48(12):1915-24.

166. Wondergem M, van der Zant FM, van der Ploeg T, Knol RJ. A literature review of 18F-fluoride PET/CT and 18F-choline or 11C-choline PET/CT for detection of bone metastases in patients with prostate cancer. Nucl Med Commun. 2013;34(10):935-45.

167. Coleman R, Hadji P, Body JJ, Santini D, Chow E, Terpos E, et al. Bone health in cancer: ESMO Clinical Practice Guidelines. Ann Oncol. 2020;31(12):1650-63.

168. Hofman MS, Lawrentschuk N, Francis RJ, Tang C, Vela I, Thomas P, et al. Prostate-specific membrane antigen PET-CT in patients with high-risk prostate cancer before curative-intent surgery or radiotherapy (proPSMA): a prospective, randomised, multicentre study. Lancet. 2020;395(10231):1208-16.

169. Chavoshi M, Mirshahvalad SA, Metser U, Veit-Haibach P. (68)Ga-PSMA PET in prostate cancer: a systematic review and meta-analysis of the observer agreement. Eur J Nucl Med Mol Imaging. 2022;49(3):1021-9.

170. Giesel FL, Hadaschik B, Cardinale J, Radtke J, Vinsensia M, Lehnert W, et al. F-18 labelled PSMA-1007: biodistribution, radiation dosimetry and histopathological validation of tumor lesions in prostate cancer patients. Eur J Nucl Med Mol Imaging. 2017;44(4):678-88.

171. Pattison DA, Debowski M, Gulhane B, Arnfield EG, Pelecanos AM, Garcia PL, et al. Prospective intra-individual blinded comparison of [(18)F]PSMA-1007 and [(68) Ga]Ga-PSMA-11 PET/CT imaging in patients with confirmed prostate cancer. Eur J Nucl Med Mol Imaging. 2022;49(2):763-76.

172. Dietlein F, Kobe C, Hohberg M, Zlatopolskiy BD, Krapf P, Endepols H, et al. Intraindividual Comparison of (18)F-PSMA-1007 with Renally Excreted PSMA Ligands for PSMA PET Imaging in Patients with Relapsed Prostate Cancer. J Nucl Med. 2020;61(5):729-34.

173. Georgakopoulos A, Bamias A, Chatziioannou S. Current role of PSMA-PET imaging in the clinical management of prostate cancer. Ther Adv Med Oncol. 2023;15:17588359231208960.

174. Hammes J, Hohberg M, Täger P, Wild M, Zlatopolskiy B, Krapf P, et al. Uptake in non-affected bone tissue does not differ between [18F]-DCFPyL and [68Ga]-HBED-CC PSMA PET/CT. PLoS One. 2018;13(12):e0209613.

175. Gammel MCM, Solari EL, Eiber M, Rauscher I, Nekolla SG. A Clinical Role of PET-MRI in Prostate Cancer? Semin Nucl Med. 2024;54(1):132-40.

176. Sprute K, Kramer V, Koerber SA, Meneses M, Fernandez R, Soza-Ried C, et al. Diagnostic Accuracy of (18)F-PSMA-1007 PET/CT Imaging for Lymph Node Staging of Prostate Carcinoma in Primary and Biochemical Recurrence. J Nucl Med. 2021;62(2):208-13.

177. Bailey DL, Pichler BJ, Gückel B, Barthel H, Beer AJ, Bremerich J, et al. Combined PET/MRI: Multi-modality Multi-parametric Imaging Is Here: Summary Report of the 4th International Workshop on PET/MR Imaging; February 23-27, 2015, Tübingen, Germany. Mol Imaging Biol. 2015;17(5):595-608.

178. Rasul S, Hartenbach M, Wollenweber T, Kretschmer-Chott E, Grubmüller B, Kramer G, et al. Prediction of response and survival after standardized treatment with 7400 MBq (177)Lu-PSMA-617 every 4 weeks in patients with metastatic castration-resistant prostate cancer. Eur J Nucl Med Mol Imaging. 2021;48(5):1650-7.

179. Berliner C, Steinhelfer L, Chantadisai M, Kroenke M, Koehler D, Pose R, et al. Delayed Imaging Improves Lesion Detectability in [(99m)Tc]Tc-PSMA-I&S SPECT/CT in Recurrent Prostate Cancer. J Nucl Med. 2023;64(7):1036-42.

180. Fanti S, Goffin K, Hadaschik BA, Herrmann K, Maurer T, MacLennan S, et al. Consensus statements on PSMA PET/CT response assessment criteria in prostate cancer. Eur J Nucl Med Mol Imaging. 2021;48(2):469-76.

181. Zamboglou C, Strouthos I, Sahlmann J, Farolfi A, Serani F, Medici F, et al. Metastasis-Free Survival and Patterns of Distant Metastatic Disease After Prostate-Specific Membrane Antigen Positron Emission Tomography (PSMA-PET)-Guided Salvage Radiation Therapy in Recurrent or Persistent Prostate Cancer After Prostatectomy. Int J Radiat Oncol Biol Phys. 2022;113(5):1015-24.

182. Olivier P, Giraudet AL, Skanjeti A, Merlin C, Weinmann P, Rudolph I, et al. Phase III Study of (18)F-PSMA-1007 Versus (18)F-Fluorocholine PET/CT for Localization of Prostate Cancer Biochemical Recurrence: A Prospective, Randomized, Crossover Multicenter Study. J Nucl Med. 2023;64(4):579-85.

183. Bhargava P, Ravizzini G, Chapin BF, Kundra V. Imaging Biochemical Recurrence After Prostatectomy: Where Are We Headed? AJR Am J Roentgenol. 2020;214(6):1248-58.

184. Cornford P, van den Bergh RCN, Briers E, Van den Broeck T, Cumberbatch MG, De Santis M, et al. EAU-EANM-ESTRO-ESUR-SIOG Guidelines on Prostate Cancer. Part II-2020 Update: Treatment of Relapsing and Metastatic Prostate Cancer. Eur Urol. 2021;79(2):263-82.

185. Fendler WP, Eiber M, Beheshti M, Bomanji J, Calais J, Ceci F, et al. PSMA PET/CT: joint EANM procedure guideline/SNMMI procedure standard for prostate cancer imaging 2.0. Eur J Nucl Med Mol Imaging. 2023;50(5):1466-86.

186. Hope TA, Eiber M, Armstrong WR, Juarez R, Murthy V, Lawhn-Heath C, et al. Diagnostic Accuracy of 68Ga-PSMA-11 PET for Pelvic Nodal Metastasis Detection Prior to Radical Prostatectomy and Pelvic Lymph Node Dissection: A Multicenter Prospective Phase 3 Imaging Trial. JAMA Oncol. 2021;7(11):1635-42.

187. Potretzke TA, Froemming AT, Gupta RT. Post-treatment prostate MRI. Abdom Radiol (NY). 2020;45(7):2184-97.

188. Kitajima K, Hartman RP, Froemming AT, Hagen CE, Takahashi N, Kawashima A. Detection of Local Recurrence of Prostate Cancer After Radical Prostatectomy Using Endorectal Coil MRI at 3 T: Addition of DWI and Dynamic Contrast Enhancement to T2-Weighted MRI. AJR Am J Roentgenol. 2015;205(4):807-16.

189. Chau A, Gardiner P, Colletti PM, Jadvar H. Diagnostic Performance of 18F-Fluciclovine in Detection of Prostate Cancer Bone Metastases. Clin Nucl Med. 2018;43(7):e226-e31.

190. Freitag MT, Radtke JP, Afshar-Oromieh A, Roethke MC, Hadaschik BA, Gleave M, et al. Local recurrence of prostate cancer after radical prostatectomy is at risk to be missed in (68)Ga-PSMA-11-PET of PET/CT and PET/MRI: comparison with mpMRI integrated in simultaneous PET/MRI. Eur J Nucl Med Mol Imaging. 2017;44(5):776-87.

191. Jiang J, Tang X, Pu Y, Yang Y, Yang C, Yang F, et al. The Value of Multimodality PET/CT Imaging in Detecting Prostate Cancer Biochemical Recurrence. Front Endocrinol (Lausanne). 2022;13:897513.

192. Pozdnyakov A, Kulanthaivelu R, Bauman G, Ortega C, Veit-Haibach P, Metser U. The impact of PSMA PET on the treatment and outcomes of men with biochemical recurrence of prostate cancer: a systematic review and meta-analysis. Prostate Cancer Prostatic Dis. 2023;26(2):240-8.

193. Aggarwal R, Wei X, Kim W, Small EJ, Ryan CJ, Carroll P, et al. Heterogeneous Flare in Prostate-specific Membrane Antigen Positron Emission Tomography Tracer Uptake with Initiation of Androgen Pathway Blockade in Metastatic Prostate Cancer. Eur Urol Oncol. 2018;1(1):78-82.

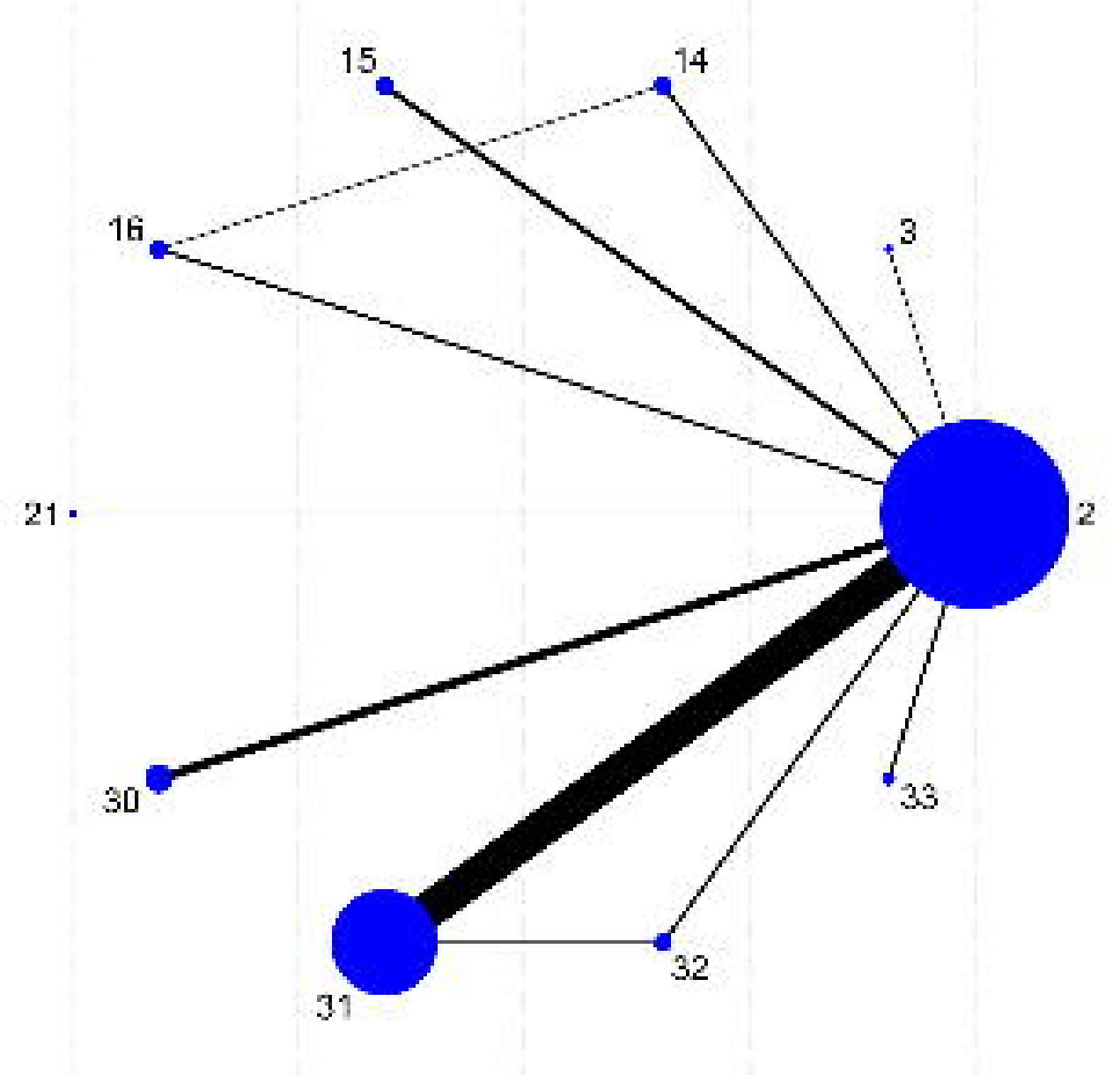
15
14
16
3
21
2
30
33
32
31

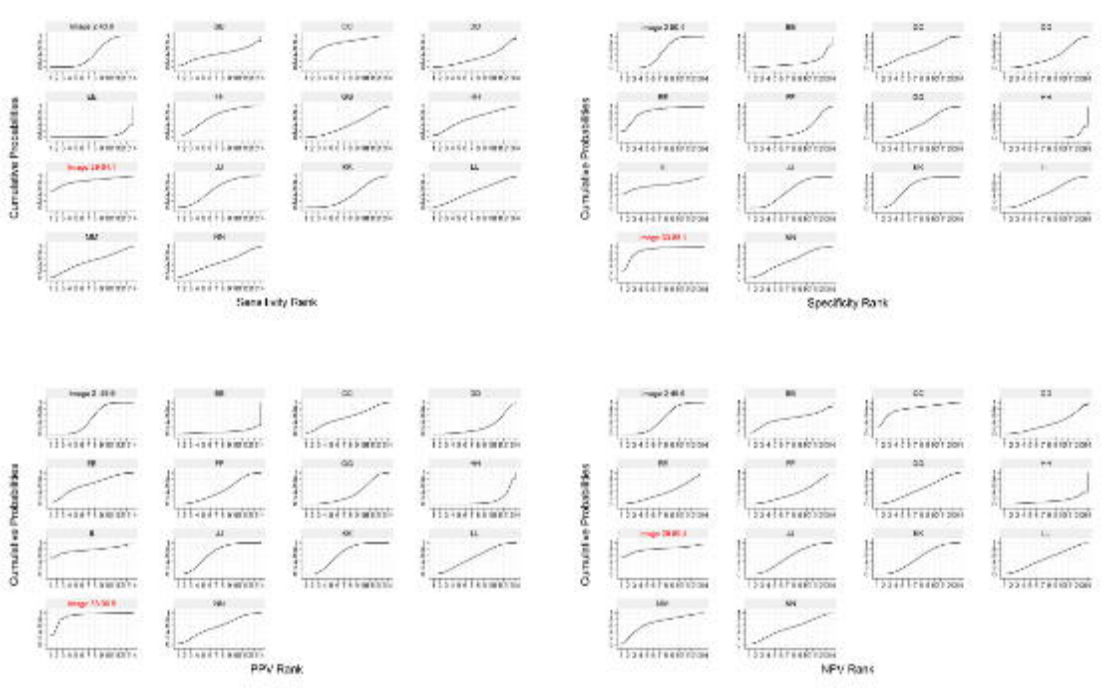
Cumulative Probabilities
Sensitivity Rank
Specificity Rank
PPV Rank
NPV Rank

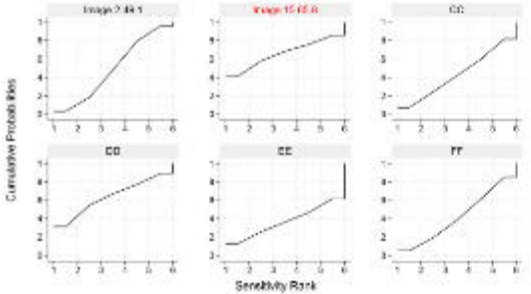
Image 2 84.1
Image 15 65.0
CC
CD
EE
FF
Cumulative Probabilities
Sensitivity Rank

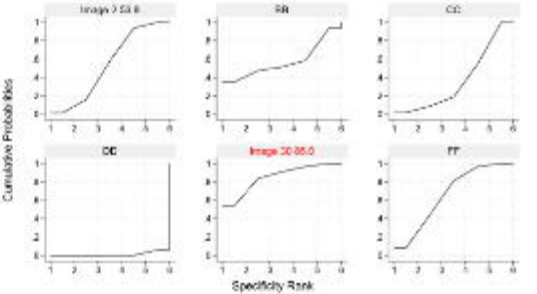
Image 2 53.8
BB
CC
CD
Image 30 85.0
FF
Cumulative Probabilities
Specificity Rank

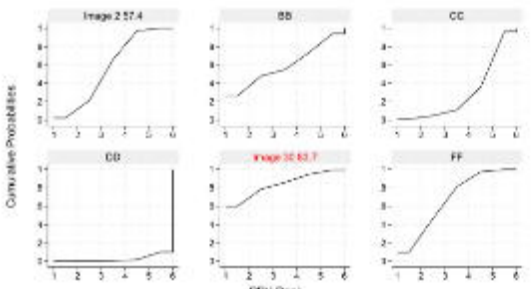
Image 2 57.4
BB
CC
CD
Image 30 83.7
FF
Cumulative Probabilities
PPV Rank

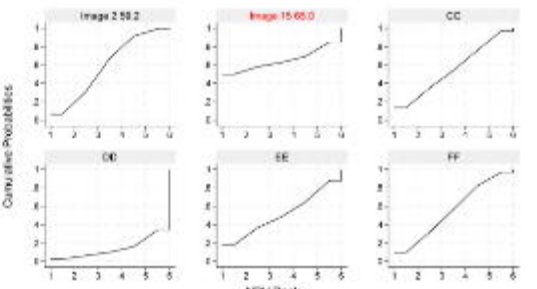
Image 2 59.2
Image 15 65.0
CC
CD
EE
FF
Cumulative Probabilities
NPV Rank

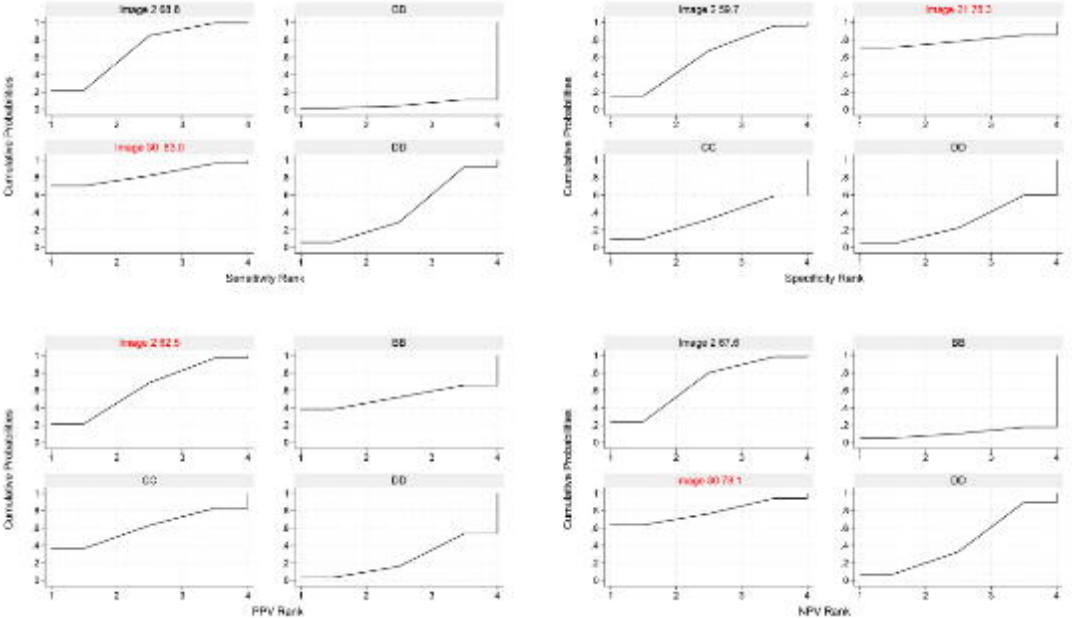
Image 2 63.6
CD
Image 90 83.0
DD
Image 2 59.7
Image 21 73.3
CC
DD
Image 2 62.5
BB
CC
DD
Image 2 67.6
BB
Image 90 79.1
DD
Cumulative Probabilities
Sensitivity Rank
Specificity Rank
PPV Rank
NPV Rank

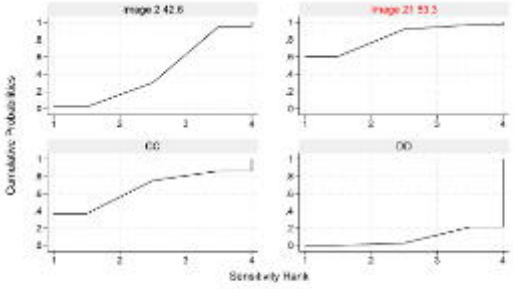
Image 2 42.6
Image 21 53.3
CC
DD
Cumulative Probabilities
Sensitivity Rank

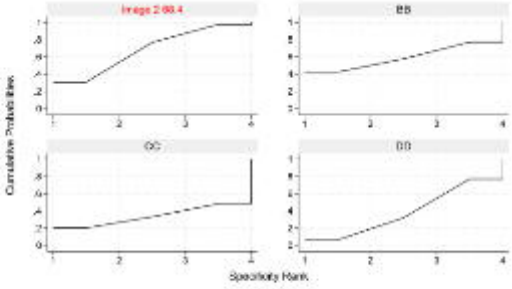
Image 2 66.4
BB
CC
DD
Cumulative Probabilities
Specificity Rank

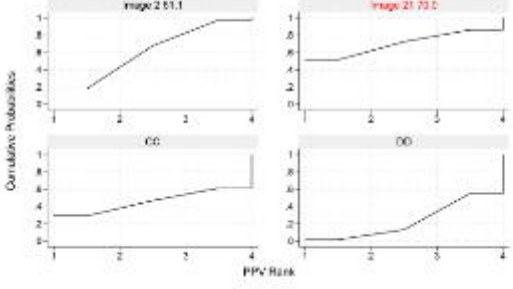
Image 2 51.1
Image 21 70.0
CC
DD
Cumulative Probabilities
PPV Rank

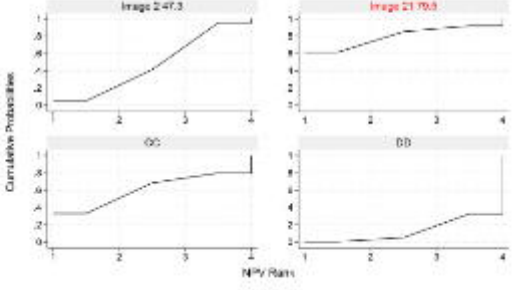
Image 2 47.3
Image 21 79.0
CC
DD
Cumulative Probabilities
NPV Rank

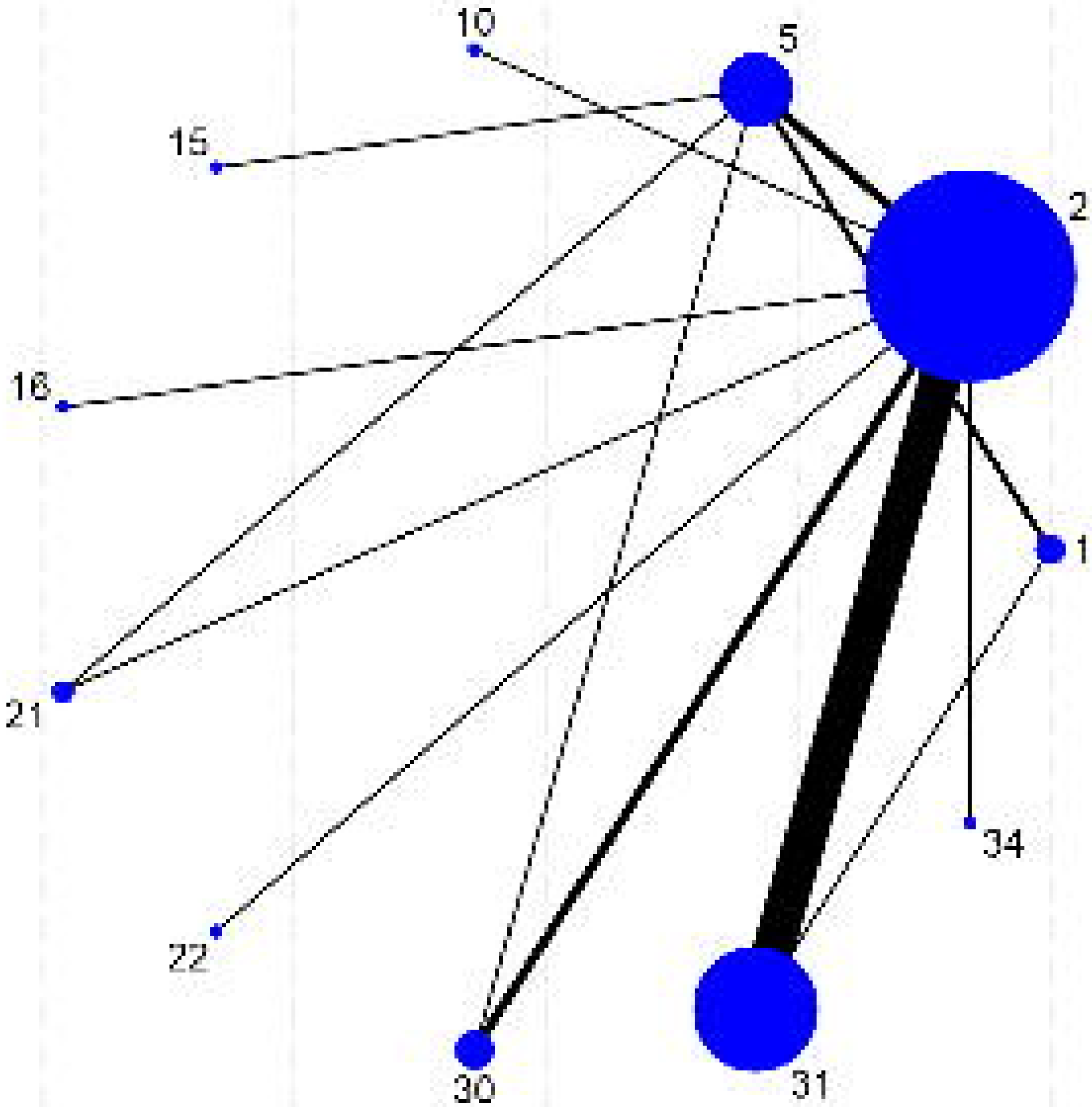
10
5
15
2
16
1
21
34
22
30
31

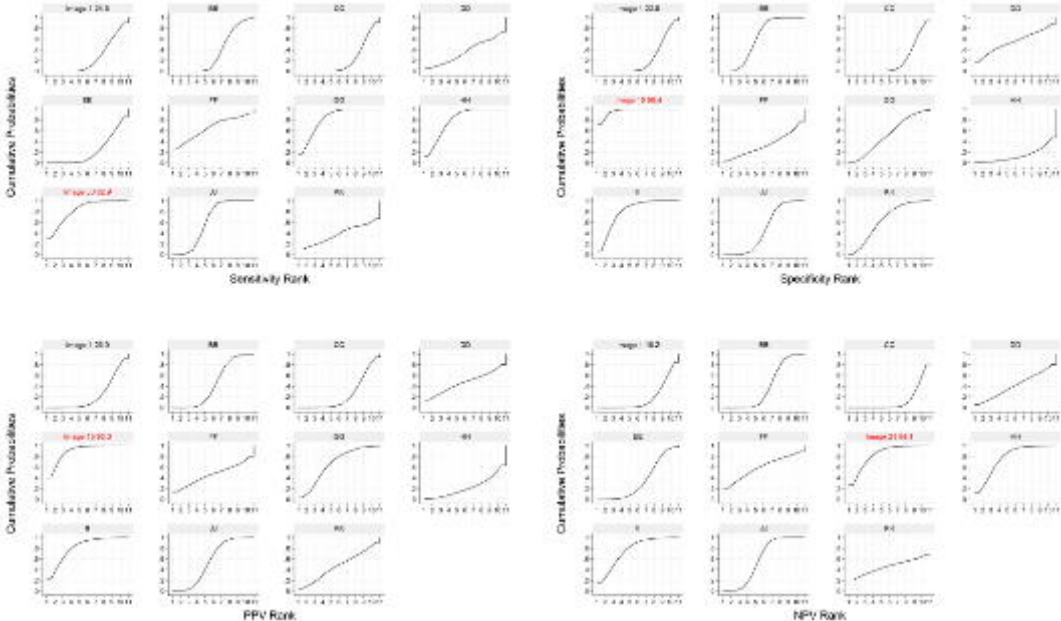
Cumulative Probabilities
Sensitivity Rank
Specificity Rank
PPV Rank
NPV Rank

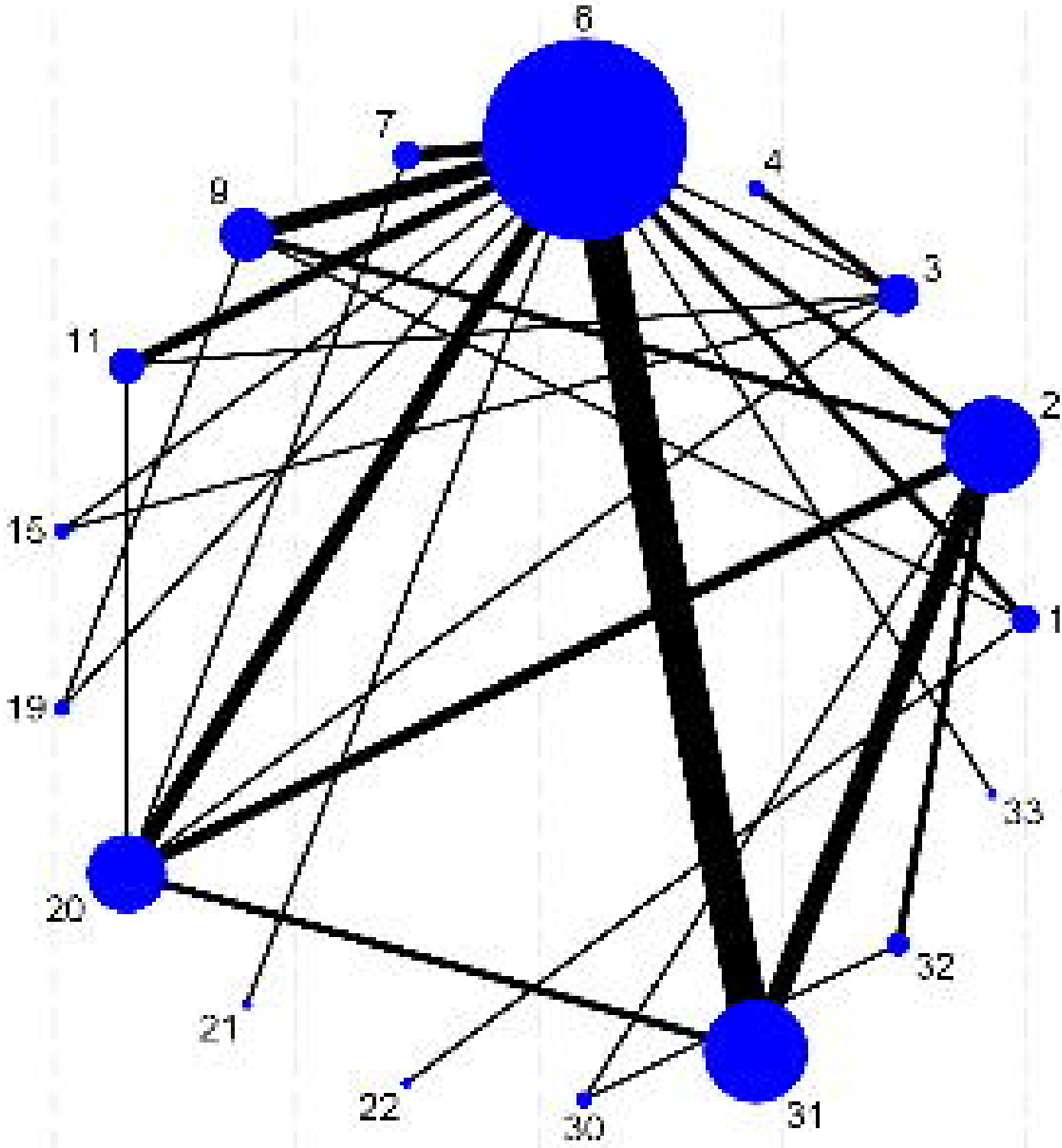
6
7
4
9
3
11
2
15
1
19
33
20
32
21
22
30
31

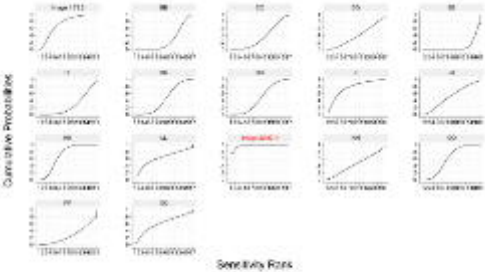
Cumulative Probabilities
Sensitivity Rank

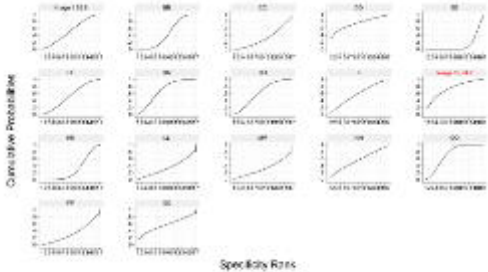
Cumulative Probabilities
Specificity Rank

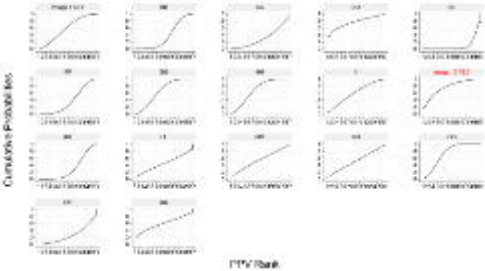
Cumulative Probabilities
PPV Rank

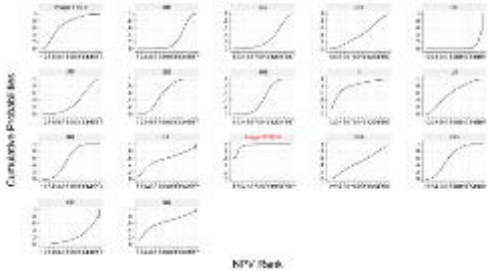
Cumulative Probabilities
NPV Rank

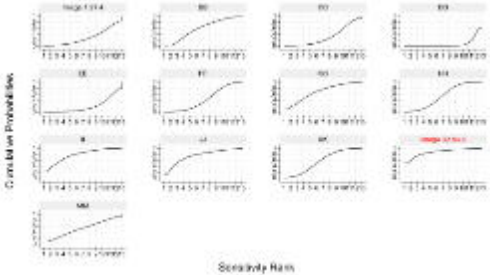
Cumulative Probabilities
Sensitivity Rank

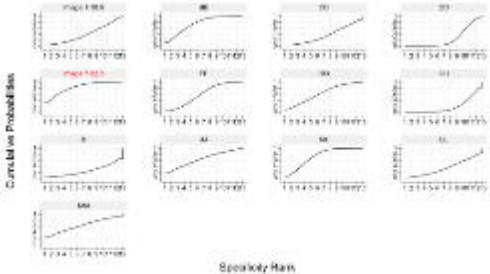
Cumulative Probabilities
Specificity Rank

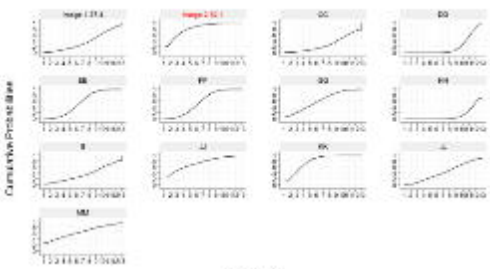
Cumulative Probabilities
PPV Rank

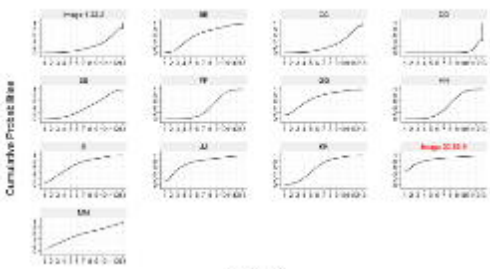
Cumulative Probabilities
NPV Rank

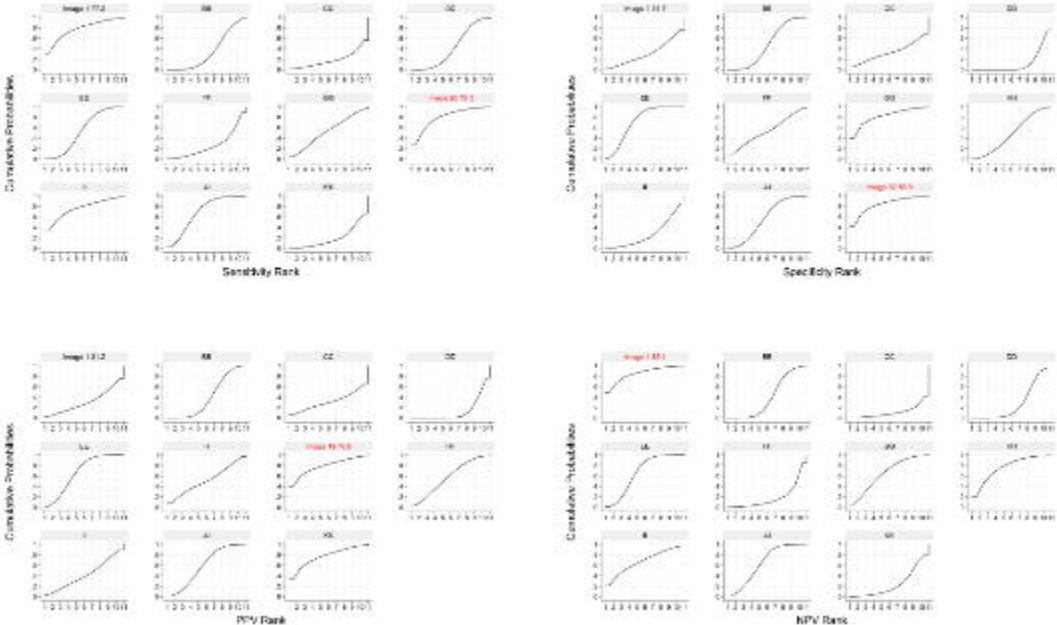
Cumulative Probabilities
Sensitivity Rank
Specificity Rank
PPV Rank
NPV Rank

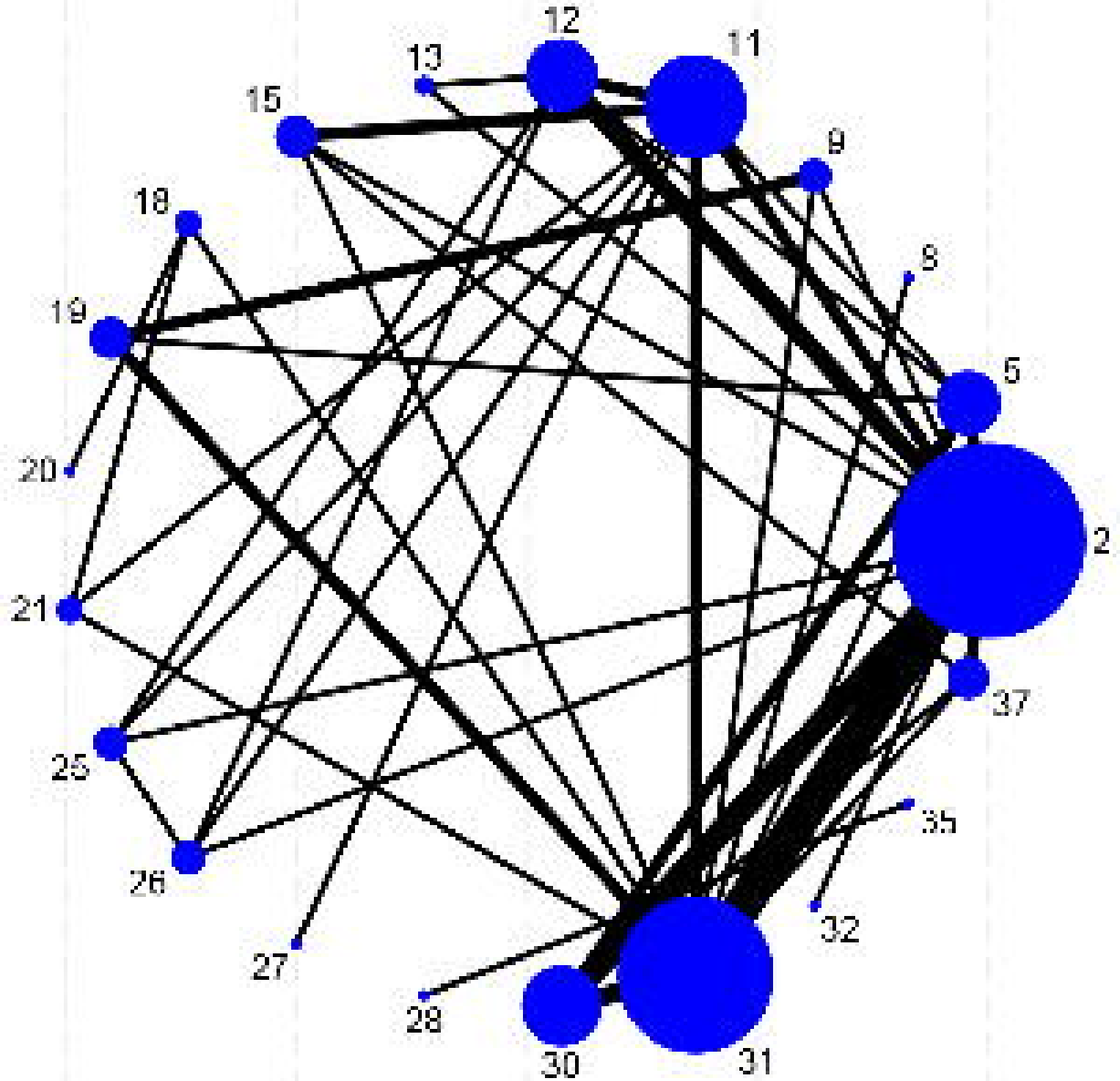
12
11
13
15
9
18
8
19
5
20
2
21
37
25
35
26
32
27
28
30
31

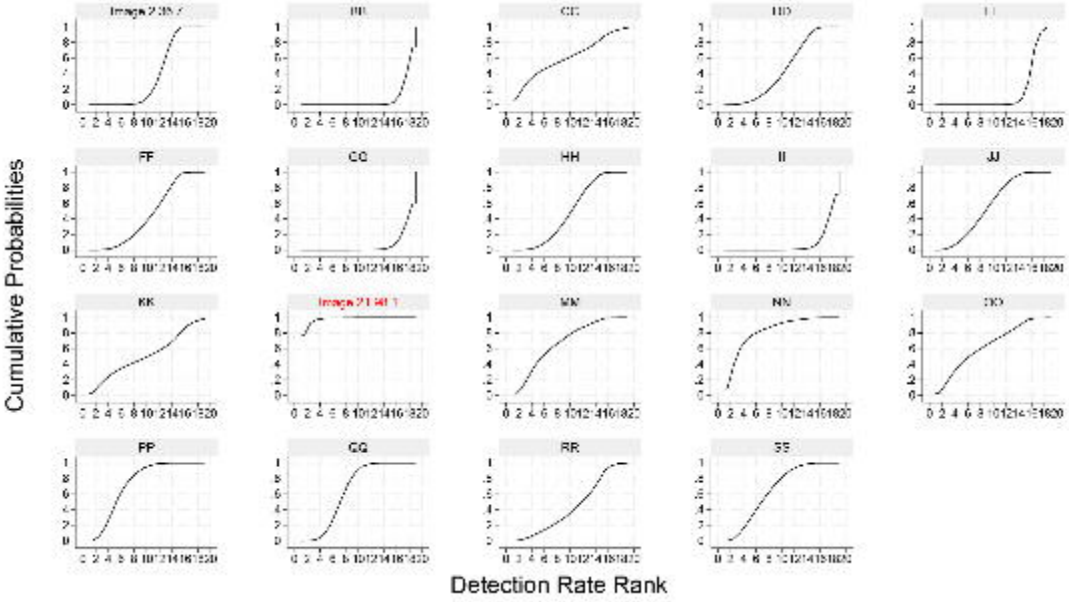
Cumulative Probabilities
Detection Rate Rank
FF
CC
HH
II
JJ
KK
MM
NN
OO
PP
QQ
RR
SS

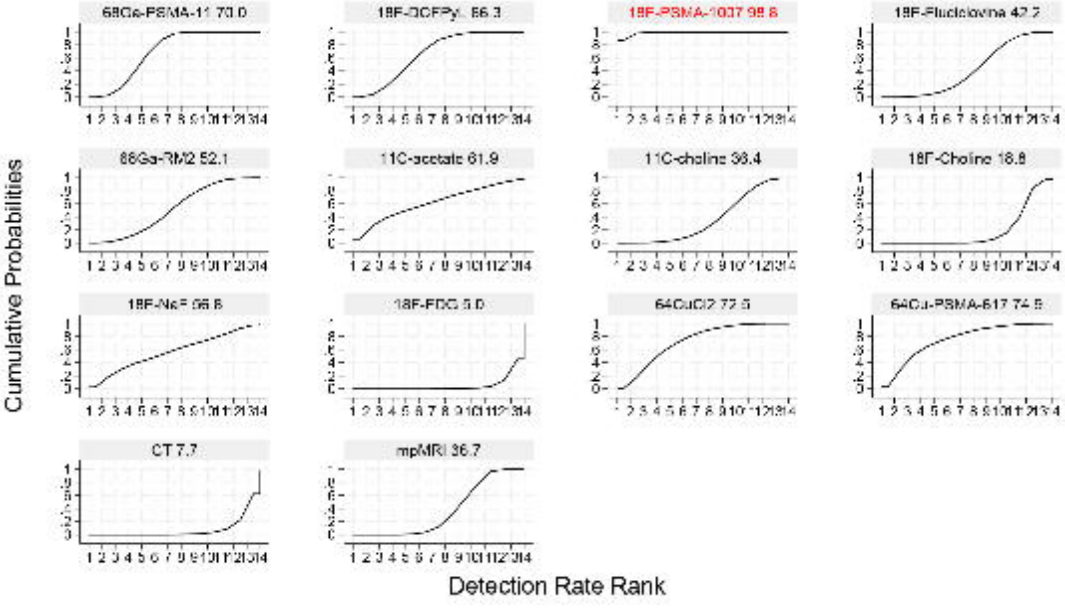
68Ga-PSMA-11 70.0
18F-DCFPy 66.3
18F-PSMA-1007 98.6
18F-Fluciclovine 42.2
68Ga-RM2 52.1
11C-acetate 61.9
11C-choline 36.4
18F-Choline 18.8
18F-NaF 66.6
18F-FDG 5.0
64CuCl2 72.5
64Cu-PSMA-617 74.5
CT 7.7
mpMRI 36.7
Cumulative Probabilities
Detection Rate Rank